Crushing Performance of Auxetic Tubes under Quasi-Static and Impact Loading

Milad Oloumi Doudaran[1], **Hamed Ahmadi** [1*], **GholamHossein Liaghat**[1,2]

[1] Faculty of Mechanical Engineering, Tarbiat Modares University, Tehran, Iran.

[2] School of Mechanical & Aerospace Engineering, Kingston University, London, United Kingdom.

(*corresponding author: Hamed Ahmadi, Faculty of Mechanical Engineering, Tarbiat Modares University, Jalal Highway, Tehran, Iran. Email: h_ahmadi@modares.ac.ir)

ABSTRACT

The aim of this paper is to investigate the energy absorption behavior of some reticulated tubes with different auxetic and non-auxetic wall grid patterns. Re-entrant, Arrow-head and Anti-tetrachiral were the three types of cellular patterns for auxetic reticulated tubes and the conventional Honeycomb pattern was used for the non-auxetic tubes. All of the designed specimens were fabricated by laser rotary cutting machine on steel tubes and the crushing tests were performed by a universal testing machine and drop weight machine for quasi-static and impact loading rates, respectively. Also, the hollow reticulated tubes were filled with Polyurethane foam to investigate the effect of filler on the crushing behavior of these novel tubes. Peak force, mean force, crushing force efficiency, total absorbed energy and specific absorbed energy were used as evaluating parameters. The results illustrate that the auxetic tubes showed a significant increase in SEA, CFE, and EA parameters compared to non-auxetic conventional structures. Foam filling of the structures caused symmetric deformation and shows the benefit of auxetic pattern even in quasi static loading. Also, a numerical analysis was carried out to simulate the experimental tests and a comprehensive discussion

is performed and based on the validation of the FE model versus the experimental crushing response the parametric study was conducted to understand further the effects of various loading rates.

Keywords: Auxetic Tube, Axial Crushing test, Impact Loading, Polyurethane Foam, Energy Absorption.

1 Introduction

In recent years, with the progress of technology, development in the designing of engineering structures for gaining novel structures with high stiffness and strength and significant weight savings increased in the industry of automotive, aerospace, and other industries. This significant work has important consequences such as passive safety, fuel consumption, etc. [1], [2]. Therefore, researchers tend to design novel and lightweight structures to improve the safety of the vehicles without increasing the weight [1]. One of the most important structures used as crash protection systems is thin-walled tubular structures that convert kinetic energy into irreversible plastic deformation [3], [4]. In designing these structures, geometric parameters and material properties should be fully considered so that the crash absorber has good damping energy [3]. Considering the above criteria, many studies on the crashworthiness parameters of thin-walled tubes, including the cross-sectional area of the tubes, including square [5], circular [6], conical [7], elliptical [8], or the effect of wall thickness, tube diameter and etc, has been done [9]. One of the novel parameters that has

been slightly tested on thin-walled tubes is the effect of auxetic units on tube's wall [1], [10], [11]

Conventional materials and structures shrink in the lateral direction when elongating in the axial direction under tensile load. The ratio between lateral and axial direction strain is defined as the Poisson's ratio (PR) [12]. These materials and structures have a positive Poisson's ratio (PPR) [12]. In contrast, some of the structures and materials under this condition have a negative Poisson's ratio (NPR) that is named auxetic structure (**Fig. 1**) [1], [2], [10], [12]. To date, a variety of auxetic structures with different deformation mechanisms have been designed and investigated, which reentrant [2], arrowhead [13] and anti-tetrachiral [14] are the most applicable and famous of them (**Fig. 2**) . As mentioned, thin-walled structures as a kind of the typical energy absorbers, have been widely used in automotive, aerospace, and other industries. Due to their excellent energy absorption capacity and extraordinary lightweight [15]. Experimental studies have shown that three modes of deformation may occur in axial loading of the thin-walled circular tubes, including axisymmetric deformation, non-axisymmetric deformation, and a mixed-mode. The deformation mode depends on the ratios of diameter to thickness and diameter to height; while the energy absorption capacity is more in the axisymmetric mode than the non-axisymmetric mode of deformation. Energy absorption typically occurs by progressive local buckling of the tubes, and the corresponding load has an fluctuated nature [3], [16]. While, in circular tubes with the auxetic wall, researches have shown that after applying a compressive displacement, the shrinkage of tube's cross-section was occurred and this shrinkage caused the stiffening of auxetic units [12]. Moreover, increasing the compressive displacement and stiffening caused strengthening of the structure [17–19]. Studies have

shown that energy absorption in auxetic structures depends on the loading velocity and loading mode [12]. Researches have shown that due to the negative Poisson's ratio in auxetic structures, structural deformation behavior in quasi-static loading is different from impact condition [20]. Cylindrical auxetic structures in low-velocity impact conditions not only showed higher specific energy absorption but also had substantially lower acceleration during the impact process due to the densification effect [1]. However, there are some shortcomings in auxetic structures. Yongguang Guo et al. [11] examined the auxetic tube. They showed that the auxetic tube has an asymmetric collapse at some loading rates. Porous materials such as polyurethane foam are used as a filler to improve the stability of crash and collapse mode of auxetic structures [3]. Researches have shown that foam energy absorption is directly related to foam density [4], [21].

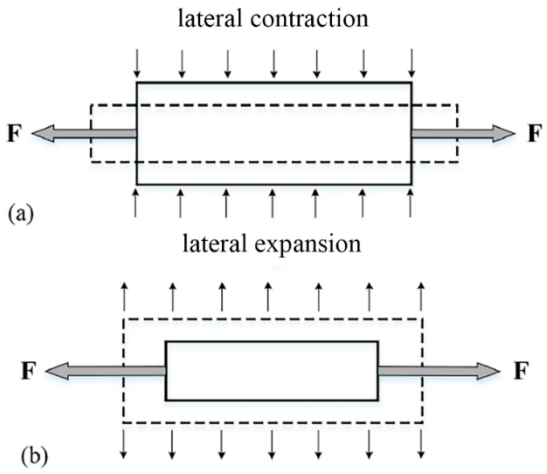

Fig. 1. Schematic diagrams of (a) conventional materials with a positive Poisson's ratio and (b) Auxetic materials with a negative Poisson's ratio under tensile loading [2].

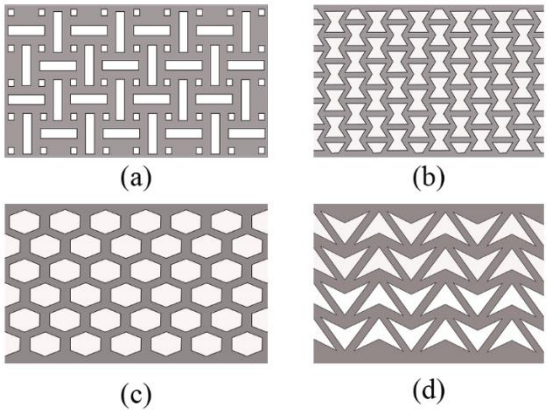

Fig. 2. Typical 2D topologies for auxetic and non-auxetic structures: (a) Anti-tetrachiral structure, (b) reentrant structure, (c) Honeycomb structure, (d) Arrowhead structure [2].

Due to the advantages of auxetic structures, researchers have been trying to design more pattern of them since the 1980s [10]. In 1982, Gibson et al. [22] presented the first two-dimensional cell structure with a negative Poisson's ratio in the form of the reentrant pattern. The introduction of the first auxetic material dates back to 1987 when Lakes [23] reported the behavior of the first foam structures with a negative Poisson's ratio. Mohsenizadeh et al. [24] examined a thin-walled cylindrical structure filled with auxetic foam and found that the energy absorption in a cylindrical structure with an auxetic foam core was higher than in a structure with a conventional foam core. Xiang YuZhang et al. [25] investigated the auxetic tubular structure with tunable stiffness. They showed the compression process of tubular structure with tunable stiffness exhibited four distinct stages (elastic, stiffness change, densification and buckling). Liu et al. [18] compared the energy absorption performances of the re-entrant auxetic and honeycomb. Hou et al. [17] examined in-plane dynamic crushing behavior of a re-entrant structure with a conventional structure. They showed that auxetic cells are responsible for the superiority of this structure in impact loading. Guo et al. [26]

analyzed the double-arrowhead structure. They found that improvements in collapse, plateau stress, and impact resistance depended on the crushing velocity. Some other studies have been done on the double-arrowhead structure. The results showed that these structures' crushing strength and Poisson's ratio were related to the velocity and compressive strain rate. As the strain rate and velocity increased, the structures became more auxetic and stronger [27], [28]. In order to study the effect of strain rate on porous structures, Nejc Novak et al. [29] investigated the Crushing Behavior of Auxetic Structures under high strain rate condition. Therefore, they fabricated and examined the high porosity (Honeycomb structure) and low porosity structures (Reentrant structure) under high strain rate loading. They observed in the case of specimens oriented with the high porosity the plateau stress increases with increasing deformation while in the case of specimens oriented with the low porosity the fluctuations at the smaller strains are larger in comparison to the specimens oriented with the high porosity. They concluded the inclination and declination of the plateau stress can be predefined by the specimen orientation. Matej Borovinšek et al. [30] examined the low-density aluminum foam under high-velocity impact loading. They inferred the aluminum foam samples deform only in the region contacting the rigid wall during impact, due to the high impact velocity; the inertial effects dominate the deformation process. Wonjoo Lee et al. [12] investigated auxetic cylindrical thin-walled structures under the low-velocity impact. They showed that the auxetic tubes had a superior specific energy absorption at low velocity impact compared to conventional structures.

As a result, few studies have been performed on the auxetic tubes. These few studies have also examined common structures such as Reentrant and Arrowhead units on tubes wall[12], [28]. While exist a lot of famous 3D auxetic structures that shows superior properties in anti-

impact field. Nejc Novaka et al. [14] investigated 3D Anti-tetrachiral structures' energy absorption under quasi-static and low-velocity impact loading. They concluded at the 3D Anti-tetrachiral structure, A significant effect of higher loading velocities observed characterized by evaluating the specific energy absorption and specific strength. However, there are some drawbacks to auxetic tubes, Yongguang Guo et al. [11] Examined the auxetic tube with the Reentrant pattern and They showed that the Reentrant auxetic tube had an asymmetric collapse at some loading rates. There are many solutions to this shortcoming such as foam filling [31]. In order to eliminate the instability of the collapse of auxetic tube, Hui ChenLuo et al. [32] Studied the structures filled with auxetic foam with considering the asymmetric collapse of the auxetic tubes. They showed that the foam filling prevented lateral buckling of auxetic tubes. Xin ren et al. [25] Filled the auxetic tube with foam and examined its energy absorption experimentally and numerically. The results showed that the energy absorption of the foam-filled tube was higher than the sum energy absorption of the single foam component and the auxetic tube. Although there are some studies on auxetic tubes but so far none of them have studied thin-walled auxetic steel tubes with Reentrant, Arrowhead and Anti-tetrachiral structures. Therefore, it is essential to investigate hollow tubes with novel auxetic structures in the form of singles and foam-filled under quasi-static and low-velocity impact loading from the perspective of future energy absorbers.

In order to consider the above-mentioned criteria, this paper uses steel tube and polyurethane foam as the base materials to manufacture conceptual designs of energy absorbing structures. Novel hollow tubes including auxetic and non-auxetic tubes were designed and fabricated under the influence of three-dimensional structures of Arrow-head, Reentrant, Anti-tetralchiral and Honeycomb, and porous tubes were fabricated by rotary laser apparatus. The

aim of the present study was to evaluate the energy absorption capacity of Auxetic and non-Auxetic single tubes and Foam-filled Auxetic and non-auxetic tube under quasi-static and low velocity impact loading. Quasi-static and low-velocity compression tests were carried out to evaluate the energy absorption characteristics of these tubes and based on the validation of the FE model versus the experimental crushing response the parametric study was conducted to understand further the effects of various loading rates. The optimal designs were reached by considering the Deformation mode, peak crushing force (PCF), mean crushing force (MCF), energy absorption (EA), and specific energy absorption (SEA).

2 Experimental study

2.1 Material properties

2.1.1 Steel tube

St12 steel [33] cylindrical tube with 0.9 mm thickness and 24.2 mm inner radius was used to fabricate the specimens. A tensile test was performed according to the ASTM E8/E8M standard to determine the properties of tube's material [34]. Tensile test specimens with dog-bone shapes were cut from the tube wall. The specimens were stretched with a universal machine at a constant velocity of 2 mm/min as shown in **Fig. 3**. **Fig. 4** shows the strain-stress diagram of the tested specimens and the main properties that were derived from the diagram were listed in **Table. 1**.

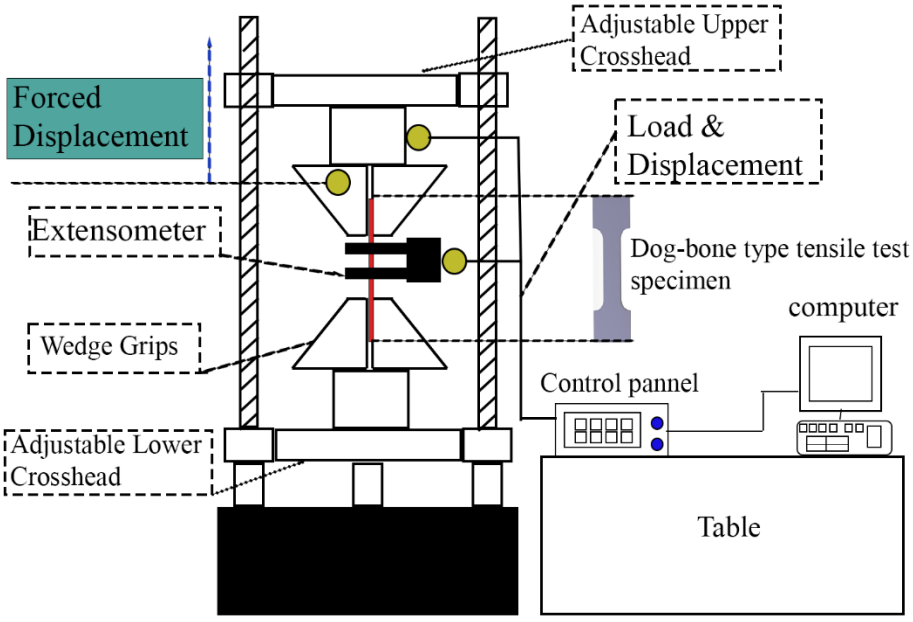

Fig. 3. The schematic of tensile test machine

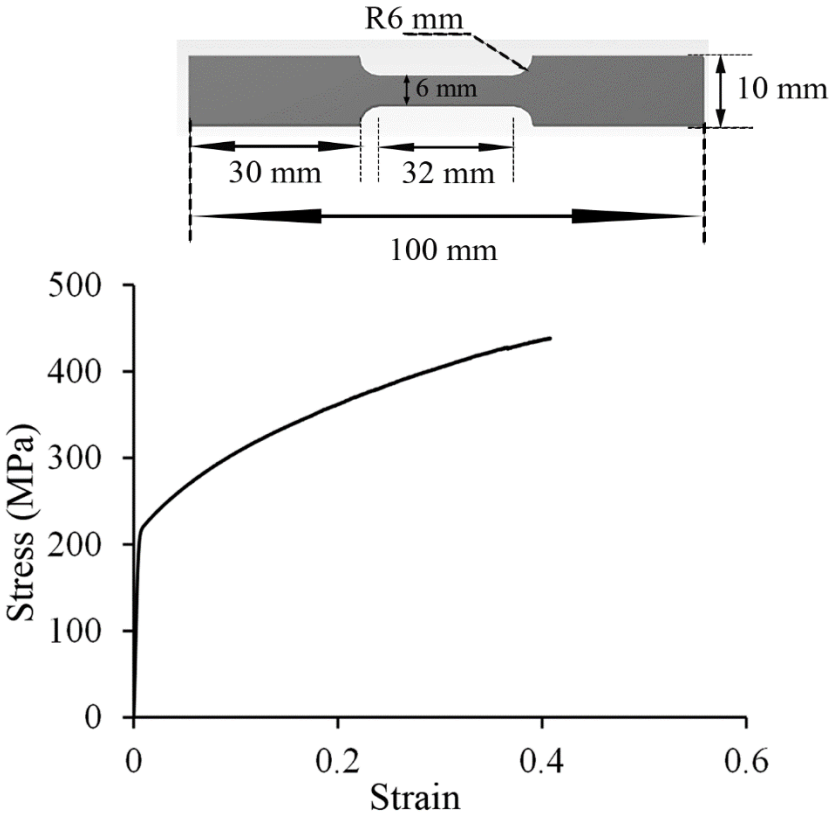

Fig. 4. Stress-Strain curves of st12 steel under tensile condition with the schematic of dog-bone specimen.

Table. 1. Properties of steel

Materials	Materials properties				
	Density (kg/m^3)	Poisson's ratio	E (GPa)	Yield stress (MPa)	Standard deviation
Steel	7800	.3	200	250	53.05

2.1.2 Polyurethane foam

Polyurethane foam is formed by the reaction between two groups of polyol and isocyanate, which on the basis of different properties and content of the constituents, flexible or rigid foams can be achieved [35]. In this study, a combination of a polyester diol with methyl diphenyl diisocyanate was used to construct crushable foam. Different combinations of these two components were mixed and pressure tests were performed on them. The most energy absorption was obtained by combining 35% diol with 65%. In the recent studies on polyurethane foam properties [36], [37], that they are similar to our study in the combination of two mentioned components, Tensile test specimens were prepared according to ASTM D 1621 standard, and pressure test specimens were prepared according to Iso 1926 standard [38]. The tests were carried out with a universal machine at a 2 mm/min velocity. Given that the foam Poisson's ratio is nearly zero [39], the engineering strain stress diagram is equal to the real strain-stress. **Fig. 5** shows the strain stress diagrams of the specimens and **Table. 2** shows the properties of the polyurethane foam.

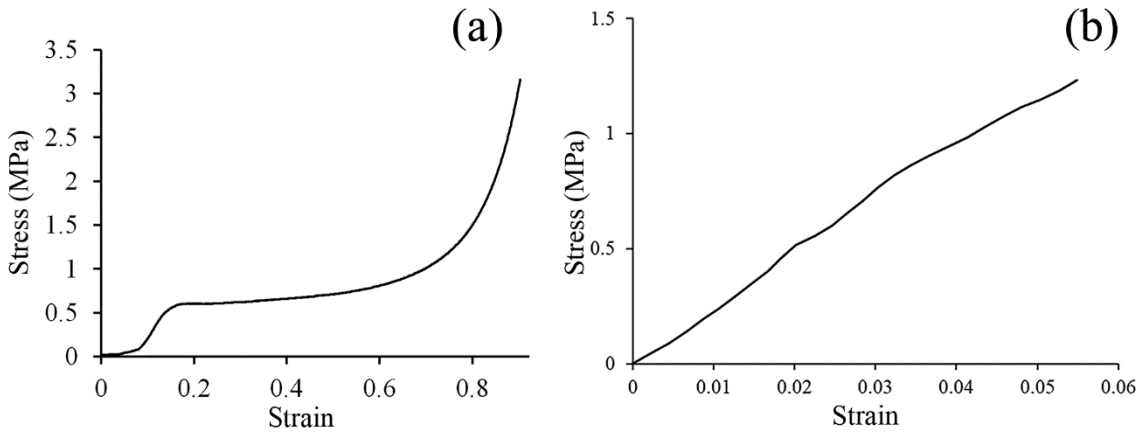

Fig. 5. Stress-Strain curves of polyurethane foam under (a) compressive and (b) tensile conditions [37].

Table. 2. Properties of polyurethane foam [37].

Materials	Materials properties					
	Density (kg/m3)	Poisson's Ratio	E_t Tensile Modulus (MPa)	E_c Compression Modulus (MPa)	Compression yield stress (MPa)	Ultimate Tensile stress (MPa)
Polyurethane foam	79	0	20	10	0.57	1.4

2.2 Design of auxetic structures

In this study 8 types of auxetic and non-auxetic tubes, with and without foam were investigated. Manufactured samples with the same dimension were labeled (see **Fig. 11-12**) in order to simplify the identification and comparison tests results. The tested specimens with their abbreviated names are shown in **Table. 3**. In order to design the specimens, symmetry in the hoop direction of the lattices' patterns should be considered. Moreover, the number of cells, the diameter and the height of the tube should be same in all of the specimens to

compare the energy absorption properties appropriately. In order to achieve the right geometries, some equations were derived according to the patterns of **Fig. 6-9**. The geometry of each cell and the space between each of them are described in each figure.

Table. 3. Abbreviated names of tubular auxetic structures

Tubes' Pattern	Reentrant	Arrowhead	Anti-tetra chiral	Honeycomb
Abbreviated names of hollow tubes	RE	AR	AC	HO
Abbreviated names of tubes filled with foam	REF	ARF	ACF	HOF

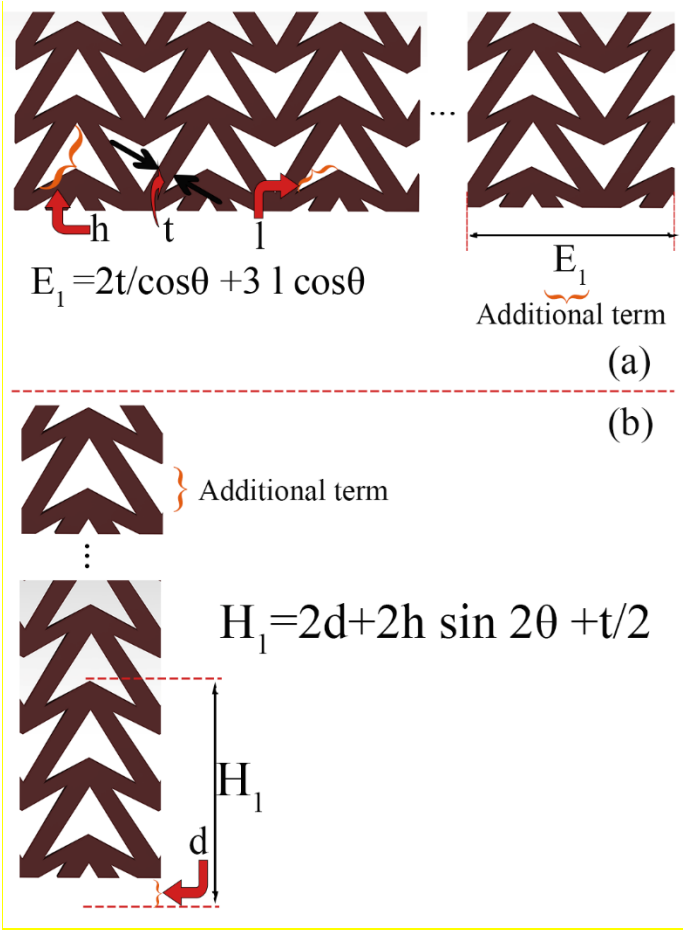

Fig. 6. The Geometric arrangement of Arrowhead auxetic units in the (a) hoop and (b) axial directions.

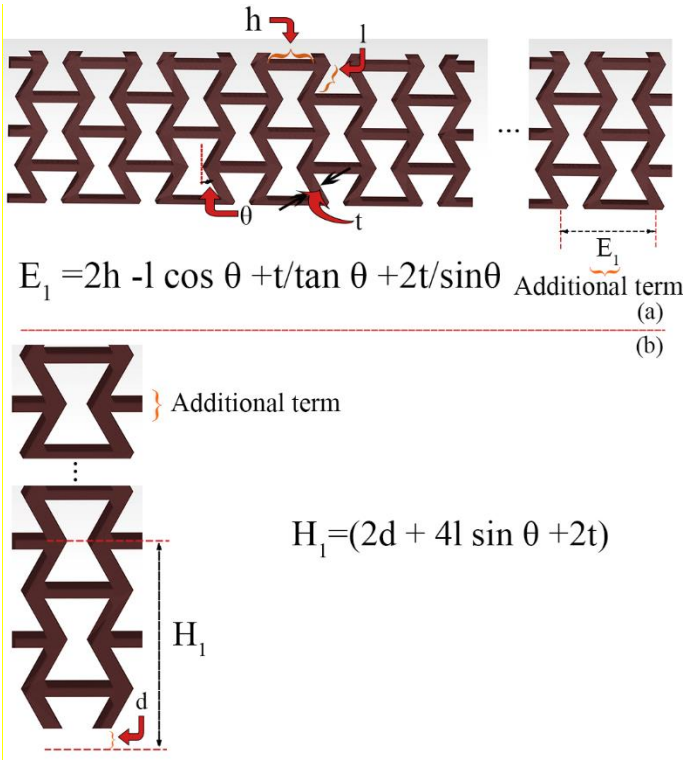

Fig. 7. The Geometric arrangement of Reentrant auxetic units in the (a) hoop and (b) axial directions.

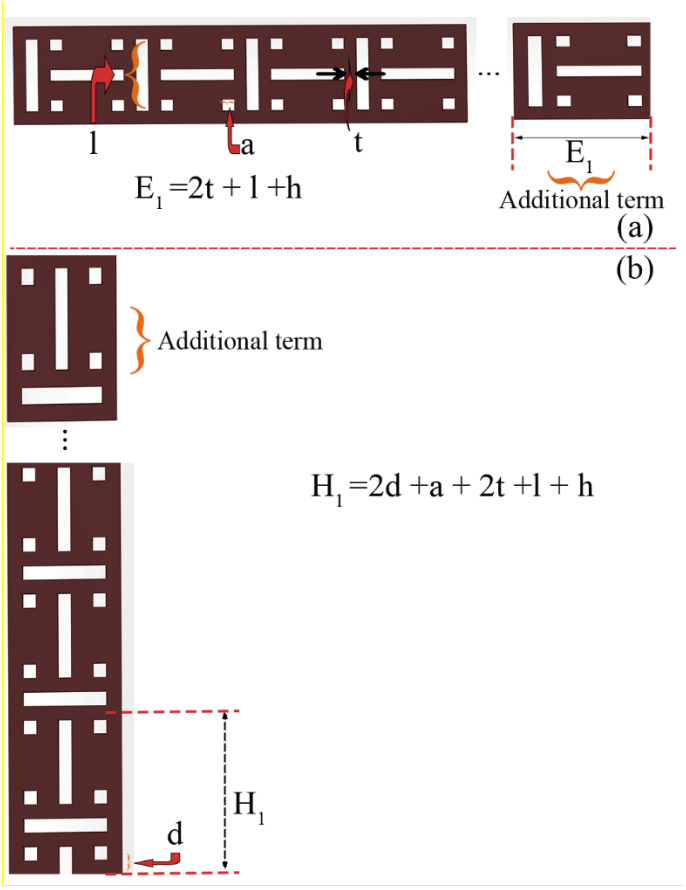

Fig. 8. The Geometric arrangement of Anti-tetra chiral auxetic units in the (a) hoop and (b) axial directions.

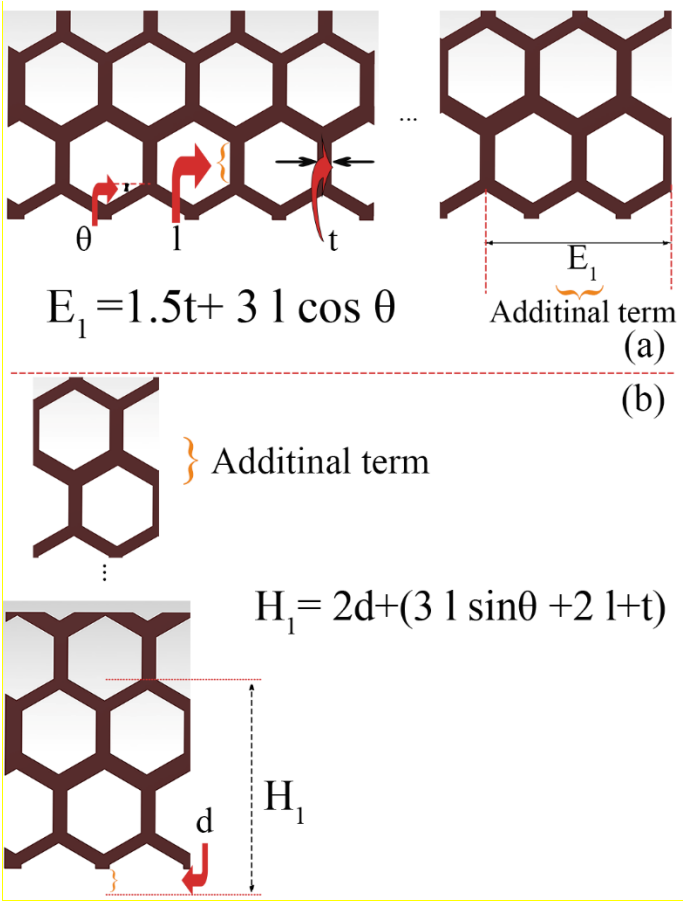

Fig. 9. The Geometric arrangement of Honeycomb non-auxetic units in the (a) hoop and (b) axial directions.

The equations 1-8 should be solved to find the central circumference (*E*) and the height (*H*) of the tubes for each pattern on the basis of geometric parameters of auxetic cells.

$$E_{AR} = k\left(\frac{2t}{\cos\theta}\right) + (2k+1)l\cos\theta \quad (1)$$

$$H_{AR} = 2d + n(2h\sin 2\theta + \frac{t}{2}) \quad (2)$$

$$E_{RE} = 2kh - (2k-1)l\cos\theta + k(\frac{2t}{\sin\theta} + \frac{t}{\tan\theta}) \quad (3)$$

$$H_{RE} = (2d + 2l\sin\theta + 2t) + n(2l\sin\theta) + (n-1)t \quad (4)$$

$$E_{AC} = k(2t + l + h) \quad (5)$$

$$H_{AC} = 2d + a + n(2t + l + h) \quad (6)$$

$$E_{HO} = k(t + 2l\cos\theta) + l\cos\theta + \frac{t}{2} \quad (7)$$

$$H_{HO} = 2d + n(3l\sin\theta + t) \quad (8)$$

In the above equations, *k* and *n* also indicate the number of cells in the hoop and axial directions. Other parameters (*t*, *l*, *d*, *h* & *θ*) are described specifically for each pattern in **Fig. 6-9**. This parameters (t, l, d, h & θ) were selected from the recent investigation on 2D auxetic structures that included reentrant, Arrowhead, Anti-tetrachiral and Honeycomb patterns [40]. Indices of *E* and *H* in each equation are the abbreviations of each pattern according to the table 3. By choosing appropriate numbers for *k* and *n*, the cell geometries would be found that *E* and *H* of each pattern be equal. **Table. 4** shows the geometric parameters obtained in this study. **Fig. 11** shows the schematic of the auxetic tubes that the overall dimension is illustrated.

Table. 4. Geometric parameters of auxetic and non-auxetic structures

Specimen	Geometric parameters							
	h (mm)	l (mm)	θ	k	n	a (mm)	t (mm)	d (mm)
RE	5.67	3.56	30	10	6	-	2.5	4.5
AR	10.67	6.53	30	9	3	-	2.5	5.5
AC	9.2	2.2	-	10	4	1.5	2	3.45
HO	-	3.76	30	16	4	-	2.8	3.08

2.3 Poisson's ratio of structures

Poisson's ratio is defined as a basic characteristic of materials as the ratio between lateral strain and axial strain, named in honor of the French scientist Simone Dennis Poisson. According to the classical theory of elasticity, for an isotropic homogeneous solid, the range

of changes in the Poisson's ratio is between -1 and 0.5. The Poisson's ratio is the one of the substantial mechanical properties, especially, in the fields of the structural stability at the macroscopic level and microstructural transitions in microscopic level [40]. The Poisson's ratio that denoted by V, is defined as the ratio of lateral strain to axial strain (see Fig.10) under axial stress and is calculated by the following equation:

$$v = \frac{\varepsilon_t}{\varepsilon_L} = \frac{\left(\frac{\Delta D}{D}\right)}{\left(\frac{\Delta L}{L}\right)} \quad (9)$$

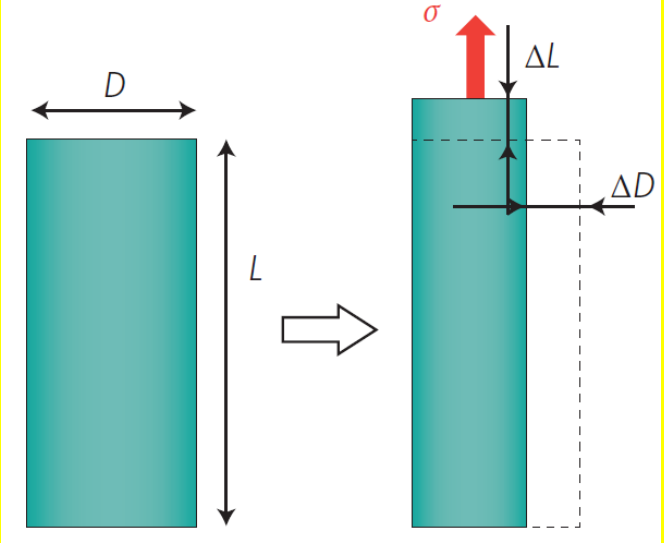

Fig. 10. Material under unidirectional axial tensile stress[40].

Since the geometric parameters of hollow structures in this study have been selected based on the study of Najafi et al. [40] Therefore, numerical calculations of Poisson's ratio of the above investigation can be relied on in this study. Accordingly, the Poisson's ratio for the hollow structures are given in **Table. 5**:

Table. 5. Poisson's ratio of 2D hollow structures calculated by FEM [40]

Structures	Reentrant	Arrowhead	Anti-tetrachiral	Honeycomb
Poisson's ratio	-0.447	-0.444	-1.603	1.106

Notice: This table is set up with FEM and the amount of Poisson's ratio is distinct from the theory.

2.4 Construction of structures

The construction of these structures requires to use of high-precision fabrication technologies. Researchers have used various methods to construct structures with complex geometries, such as the Additive manufacturing [2] or the laser cutting technology [16]. Laser cutting is one of the most widely used method for cutting metals such as steel, aluminum, etc. and have received a lot of attention [41]. The latest laser cutting technology is fiber laser cutting technology that has shown a dimensional accuracy of over 95% [42], [43]. Laser cutting is a thermal process that uses the energy produced by the laser to cut. The results showed that the effect of heat on the structure's mechanical properties was low [44].

After calculating the number of cells from above equations, these structures were designed in CATIA v5r21 software. To fabricate the structures, a 1000 W rotary fiber laser cutting machine was used. The schematic of hollow tubes are illustrated in **Fig. 11**. In order to fabricate the foam filled tubes the polyurethane foam elaborated in the previous section was poured into the tubes. **Fig. 12** shows the schematic of manufacturing process of Foam-filled

hollow tube.

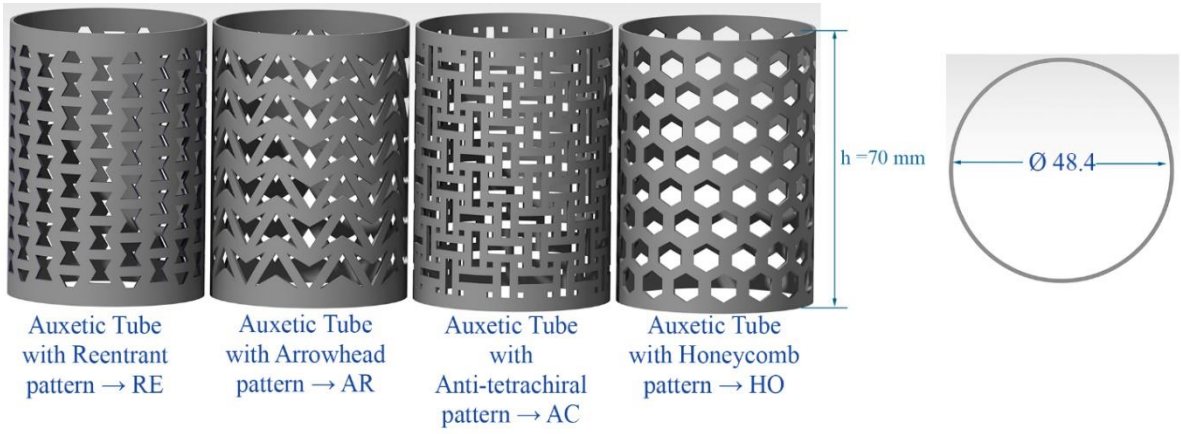

Fig. 11. The schematic of Auxetic and non-Auxetic tubes

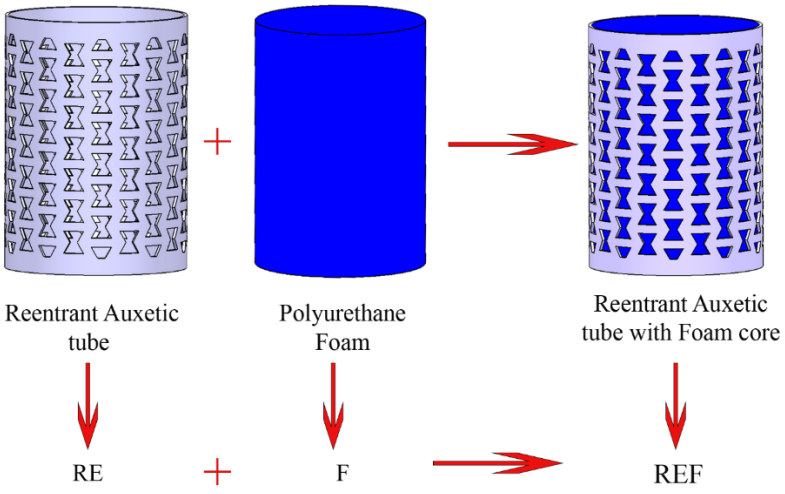

Fig.12. The schematic of manufacturing process of Foam-filled tube.

2.5 Test Setup

2.5.1 Quasi-static compressive tests

The quasi-static compressive test was performed on all of the specimens (RE, AR, AC, HO, REF, ARF, ACF and HOF structures) to study the deformation mode, load-displacement curves and energy absorption capacity of the structures. The quasi-static tests carried out with WDW-300E Universal Testing Machine (Micro Controlled Electronic Universal Testing

Machine). The specimens were subjected to a compressive axial load at a constant velocity of 5 mm/min (see **Fig. 13**). During the specimens' collapse, the upper platen moved towards the lower platen, and the load cell in the upper platen recorded the load and transmitted the information to the computer. The specimens were crushed to about 70% of their original length.

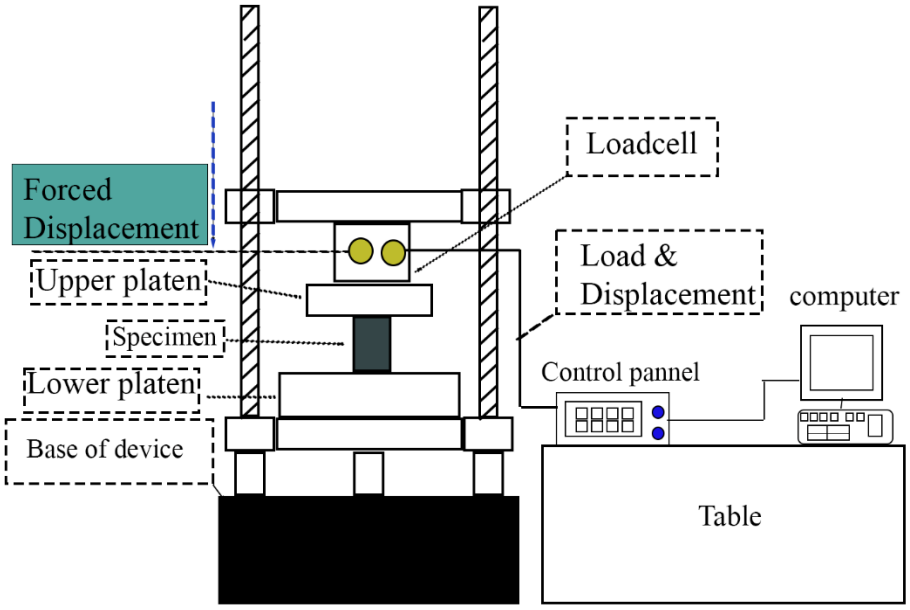

Fig. 13. The schematic of universal test machine.

2.5.2 Low-velocity impact tests

This test was performed only for empty auxetic tubes (RE, AR, AC and HO structures) to study the effect of loading rate on the response of the fabricated specimens. The tests were performed with a drop hammer machine, illustrated in **Fig. 14**. It consists of two upper and lower platens that the upper platen is connected to a variable mass moving carriage. The carriage was attached to four pillars that could move up and down with minimal friction, and the lower platen was fixed. To perform the impact test, the specimen was fixed in the lower platen and the upper platen was fall from a certain height. With considering energy absorption

of tubes on quasi-static state equal to the “1/2mv^2” equation the approximate incident velocity derived. Then with “v=√2gh” equation the height of falling weight derived. In this study, the upper platen's height was set to 30 cm, and its mass was 44.9 kg.

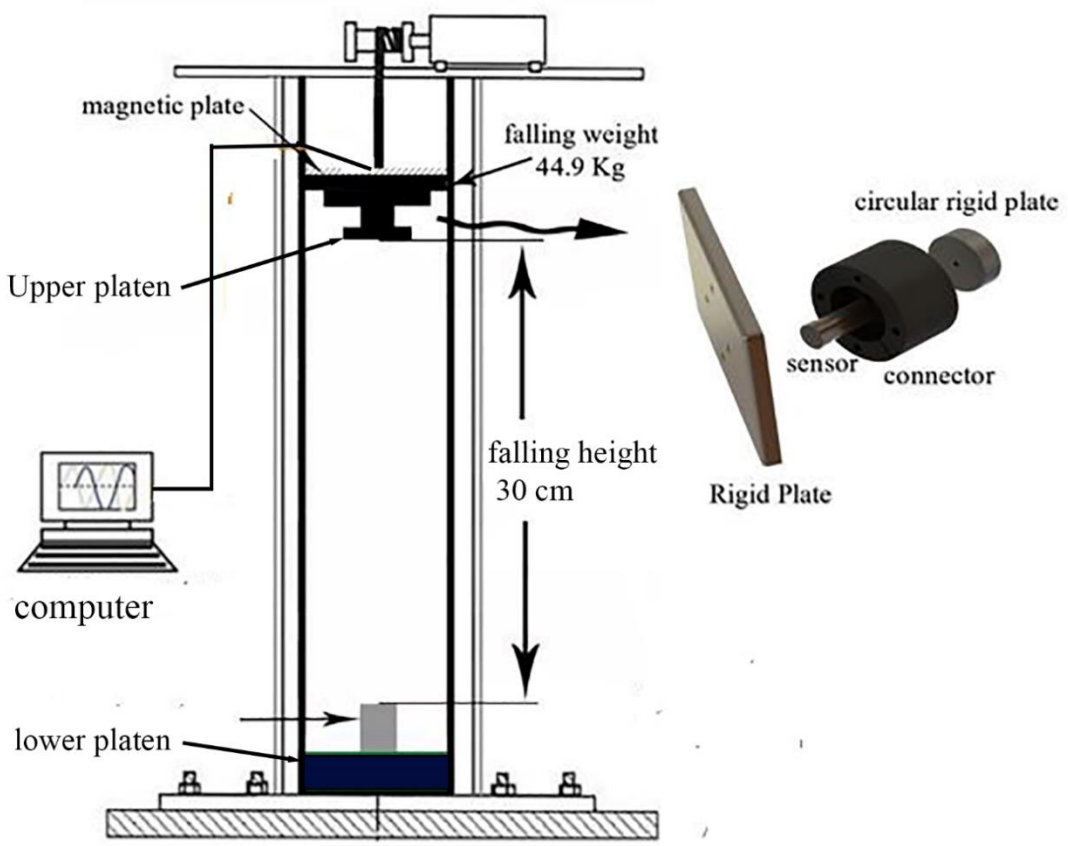

Fig. 14. The schematic of drop hammer test machine.

3 Numerical study

3.1 Finite element models

In order to learn more about the structural performance of the auxetic tubes, the FE analysis was performed using ABAQUS/Explicit. The FE model was set up for the RE, AR, AC, HO, REF, ARF, ACF and HOF structures with the same dimensions as those fabricated and

in the experiments. For hollow tubes (RE, AR, AC and HO) the solid model was discretized by three-dimensional hexahedral element (type C3D8R) were used with a mesh size of 0.5 mm and 2 elements were used through the thickness, also for foam core three-dimensional hexahedral element (type C3D8R) were used with a mesh size of 2 mm, as this provided the converged result. **Table. 7** shows the number of elements in the optimized simulation of structures. In the FE model for the quasi-static (see **Fig. 15**) tests (section 2.1), the structures were compressed between the top and the bottom rigid plates at a velocity of 1 m/s and this simulation conducted for RE, AR, AC, HO, REF, ARF, ACF and HOF structures. Moreover, in the FE model for the low-velocity impact loading (see **Fig. 16**) tests (section 2.2), the initial velocity was applied to the upper platen that the value of initial velocities presented as follows: 2.45 m/s, 4.9 m/s, 9.8 m/s, 19.6 m/s. The low-velocity impact simulation just conducted for RE, AR, AC and HO structures. General contact was set up for the structures. The friction coefficient for contacts was determined as 0.2 by using past studies [11].

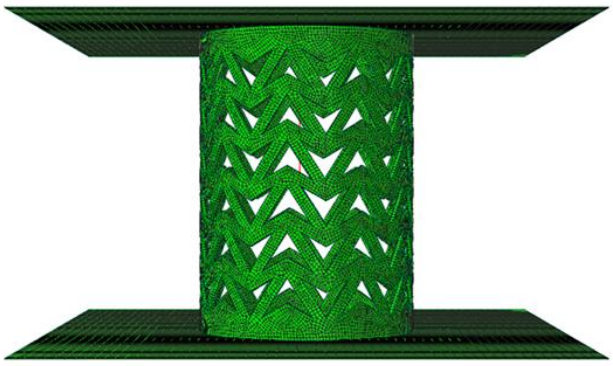

Fig. 15. The FE model for the quasi-static loading

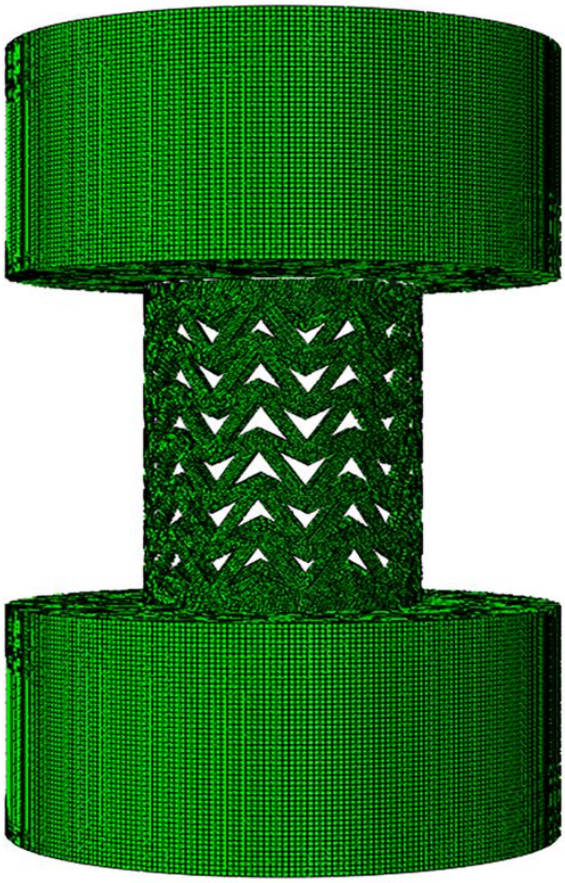

Fig. 16. The FE model for the low-velocity impact loading

Table 7 Number of solid meshes of structures for quasi-static test simulation

structures	RE	AR	AC	HO	SO
Total number of elements	64176	62346	57632	54860	88340

3.2 Material constitutive models

3.2.1 Polyurethane Foam

The "CRUSHABLE FOAM" material model with isotropic hardening in ABAQUS/Explicit was adopted to represent the crushing behaviors of the polyurethane foam with following mechanical properties: Young's modulus 20 MPa, density 0.000079 g/mm3, plastic Poisson's ratio 0, compression yield stress ratio 2.9, and yield stress 0.57 MPa.

3.2.2 Steel tube

The steel tube was modeled as an elastic-plastic material. Experimental measurements were performed to achieve the stress-strain curve according to ASTM E8 / E8M standard. **Fig. 4** shows the true stress-strain curve of a steel tube. The yield stress and ultimate stress were approximately 250 and 400 MPa, respectively. For considering strain rate effect on steel tubes, the Johnson-Cook material model was applied. On this basis, the flow stress in the plastic deformation is expressed as follows:

$$\sigma = (A + B\varepsilon^{n})(1 + C\ln\dot{\varepsilon}^{*})(1 - T^{*\,m}) \tag{10}$$

Where σ is the equivalent stress, and ε is the equivalent plastic strain. A is the yield stress of the material under reference conditions. B is the strain hardening constant, n is the strain hardening exponent, C is the strengthening coefficient of strain rate and m is the thermal softening coefficient. In the flow stress model, $\dot{\varepsilon}^{*}$ and T^{*} are as follows:

$$\dot{\varepsilon}^{*} = \frac{\dot{\varepsilon}}{\dot{\varepsilon}_{ref}} \tag{11}$$

$$T^* = \frac{T - T_{ref}}{T_m - T_{ref}} \quad (12)$$

Where $\dot{\varepsilon}^*$ is the dimensionless strain rate, T^* is the homologous temperature, T_m is the melting temperature of the material, and T is the deformation temperature. $\dot{\varepsilon}_{ref}$ and T_{ref} are the reference strain rate and the reference deformation temperature. If $T=T_{ref}$ and $\dot{\varepsilon} = \dot{\varepsilon}_{ref}$, Eq. 10 is modified as follows:

$$\sigma = (A + B\varepsilon^n) \quad (13)$$

By taking a natural logarithm from both sides of the equation, the modified equation can be obtained as shown below:

$$Ln(\sigma - A) = nLn\varepsilon + LnB \quad (14)$$

By substituting the flow stress and strain values at the reference deformation conditions from **Fig. 4** into equation 14, the linear relationship plot between ln(σ-A) and ln(ε) was drawn (**Fig. 17**). In this diagram, the line's slope represents the value of n, and the value of distance from the origin represents the value of Ln B.

Finally, it was assumed that $T = T_{ref}$, so the Eq.10 is expressed as follows:

$$\sigma = (A + B\varepsilon^n)(1 + C \ln \dot{\varepsilon}^n) \quad (15)$$

Where the values of A, B and n were obtained as mentioned above and the value of constant C was achieved from ref [45]. **Table. 8** listed the obtained parameters.

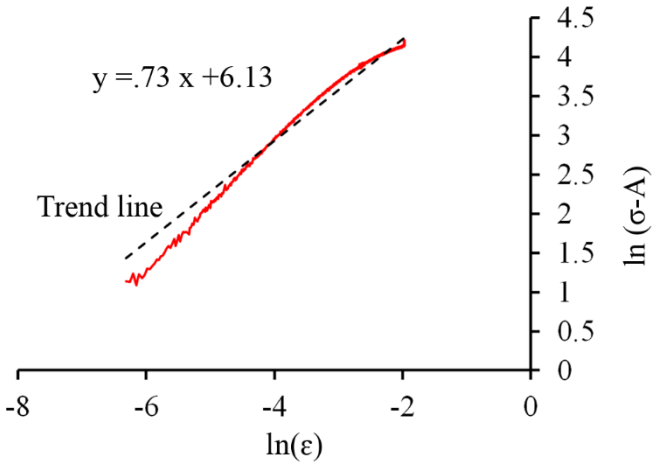

Fig. 17. Relationship between ln (σ - A) and ln ε under the reference conditions.

Table. 8. Parameters of Johnson-Cook equation

A (MPa)	B (MPa)	n	C	$\acute{\varepsilon}_0$
250	480	0.73	0.09	0.00092

3.3 Validation of FE models

Fig. 18, **Fig. 21**, **Fig. 24**, **Fig. 26, Fig. 28** and **Fig. 30**. show the comparison of Load-displacement curves and final deformation patterns of all auxetic tubes including RE, AR, AC, HO, REF, ARF, ACF and HOF structures under quasi-static loading and RE, AR, AC and HO structures under low-velocity impact loading between numerical results and experimental tests, respectively. **Table. 9-10** summarized the comparison of compression indicators between numerical results and experimental results. It was found that numerical results agreed well with experimental results.

4 Results and discussion

In this study, three different types of auxetic reticular cylindrical tubes were fabricated, tested under quasi-static and impact loading and simulated by a FEM software, ABAQUS. The results were compared with a non-auxetic reticular cylindrical tube. Also, the specimens were

filled by polyurethane foam and its effect on the failure mechanisms and energy absorbing parameters were investigated. A 300 kN universal machine was used for quasi-static loading with a rate of 5 mm/min, and the impact tests were performed with a drop hammer machine, where the impact velocity at the incident moment was 2.45 m/s. All of the tested structures were also examined by numerical simulation for further investigation.

In order to investigate the specimens, the crash parameters are calculated as follows:

First of all, the energy absorption was calculated as Eq. 16:

$$\mathrm{EA(d)} = \int_0^{\mathrm{d}} \mathrm{F(x)dx} \tag{16}$$

Where d is the crushing distance and F denotes the crushing force. The mean crushing force for a given deformation calculated as Eq. 17:

$$\mathrm{MCF} = \frac{\mathrm{EA(d)}}{\mathrm{d}} \tag{17}$$

The specific energy absorption is defined as the energy absorbed per unit mass of the structure. So it can be written as Eq. 18:

$$\mathrm{SEA(d)} = \frac{\mathrm{EA(d)}}{\mathrm{M}} \tag{18}$$

Crushing force efficiency (CFE) is defined as the ratio of the mean crushing force (MCF) to the peak crushing force (PCF) as shown in Eq. 19:

$$\mathrm{CFE} = \frac{\mathrm{MCF}}{\mathrm{PCF}} \tag{19}$$

4.1 Axial Crushing Response

In order to show the auxeticity effect on the behavior of reticulated thin-walled tube, the collapse modes (**Fig. 18**) and load-displacement diagrams (**Fig. 19**) of fabricated specimens

have been studied. The results show that the pattern of crushing and the fluctuating force during the crushing are almost different from each other. In conventional HO structures, progressive folding is observed, which occurred as a repeating pattern, and the initial fold began from the top of the structure. All the wrinkles were expanded out, so that the diameter of the densified tube was larger than the non-deformed tube. On the other hand, the collapse mode of the auxetic tubes were different. The folds in AR and AC specimens were symmetric but they were non-symmetric in RE specimens. The main point in auxetic tubes is that the folds occurred approximately 50% inwards and 50% outwards which did not expand out and the diameter did not change approximately. This behavior is the result of the negative Poisson's Ratio that causes shrinking in hoop direction and avoid the wall of the tube from large expanding out in local buckling. This type of collapsing makes the auxetic tubes stiffer during every fold of the progressive collapse, except the AR specimen. Although the tube is shrunk in the hoop direction, but the wall in the unit cell is oblique that its strength against local buckling in the axial direction is less than the other types of auxetic tubes. The other difference between auxetic tubes and non-auxetic tubes was that in auxetic structures, deformation may be occurred in above, below, or the middle of the structure. As the compressive displacement increased, the stiffening gradually increased, which strengthened the structures. But the HO specimens wrinkled from top of the tube and the load fluctuations are regular.

The load-displacement diagrams of the studied specimens are shown in **Fig. 19**. The stiffness of the structure at the beginning of the loading, before the first wrinkle, and also the load dropping after the peak load are almost the same for all of the specimens but the behavior of tubes during the crushing process are completely different. The load for HO tubes is

fluctuated regularly according to the number of symmetric wrinkles. This fluctuating was not seen in the RE diagram while the load gradually increases. This smooth load increasing is seen in the two other specimens, but irregular fluctuation is also observed.

The main evaluating parameters were listed in **Table 9**. According to the results, the peak force of RE specimens are larger than others, but the mean crushing force (MCF) of AC specimens is more than others. The maximum crushing force efficiency was about 70% for AC auxetic tube, while this parameter was obtained for RE, AR and AC structures, 33.3%, 67.6% and 41%, respectively. Therefore, in most cases, auxetic structures in the quasi-static state had a greater amount of crushing force efficiency (CFE) compared to conventional structures.

One of the main studied parameters was SEA which evaluate the performance of the crushing tube considering its weight. According to the results, although the absorbed energy of the auxetic structures are more than the non-auxetic one, but because of the lower weight of the tube, the SEA of the HO specimens are more than the others (**Fig. 20**).

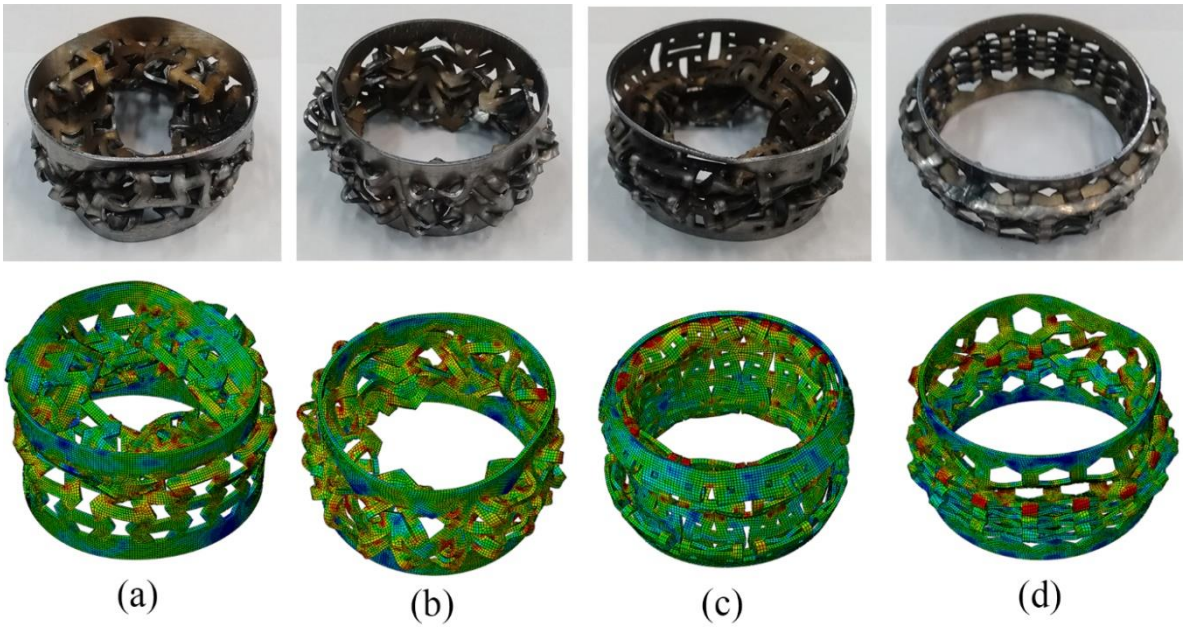

Fig. 18. Comparison of auxetic and non-auxetic tubes final deformation mode under quasi-static loading: (a) RE, (b) AR, (c) AC and (d) HO structures. (above images are experimental results and below images are numerical results).

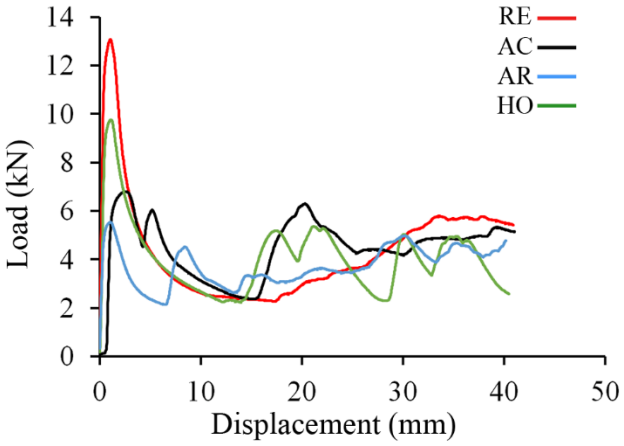

Fig. 19. comparison of Load-Displacement diagrams for RE, AR, AC and HO structures in quasi-static loading condition.

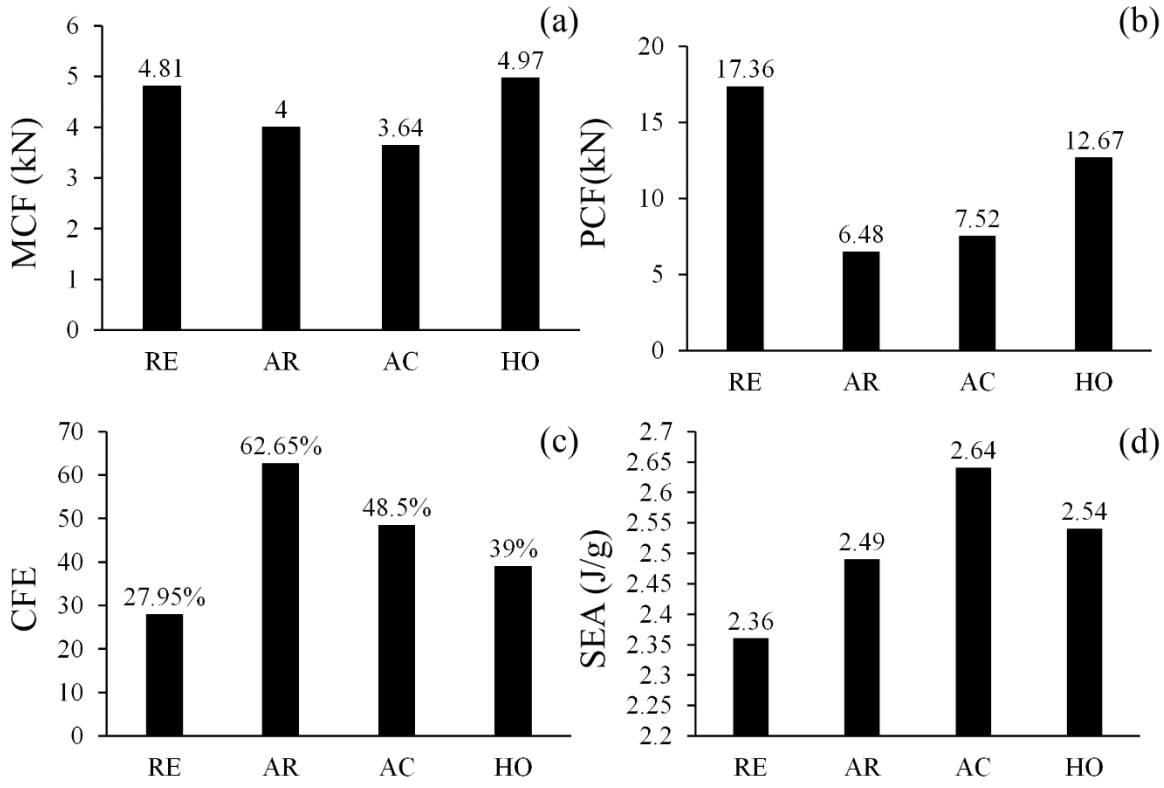

Fig. 20. Comparison of the main evaluating parameters, (a) MCF, (b) PCF, (c) CFE, (d) SEA.

As shown in **Fig. 18 & 21** and **Table. 9**, a good agreement can be observed between experimental and numerical results. So, by the aid of FE simulations more discussion about the failure mechanisms can be carried out. As indicated in **Fig. 22**, the collapse pattern observed in the experiments for the structures is also existed in numerical simulation and the simulation accurately predicts the deformation patterns and failure modes of specimens. With respect to the stress contours drawn, it is possible to identify the points where the stress concentration occurred.

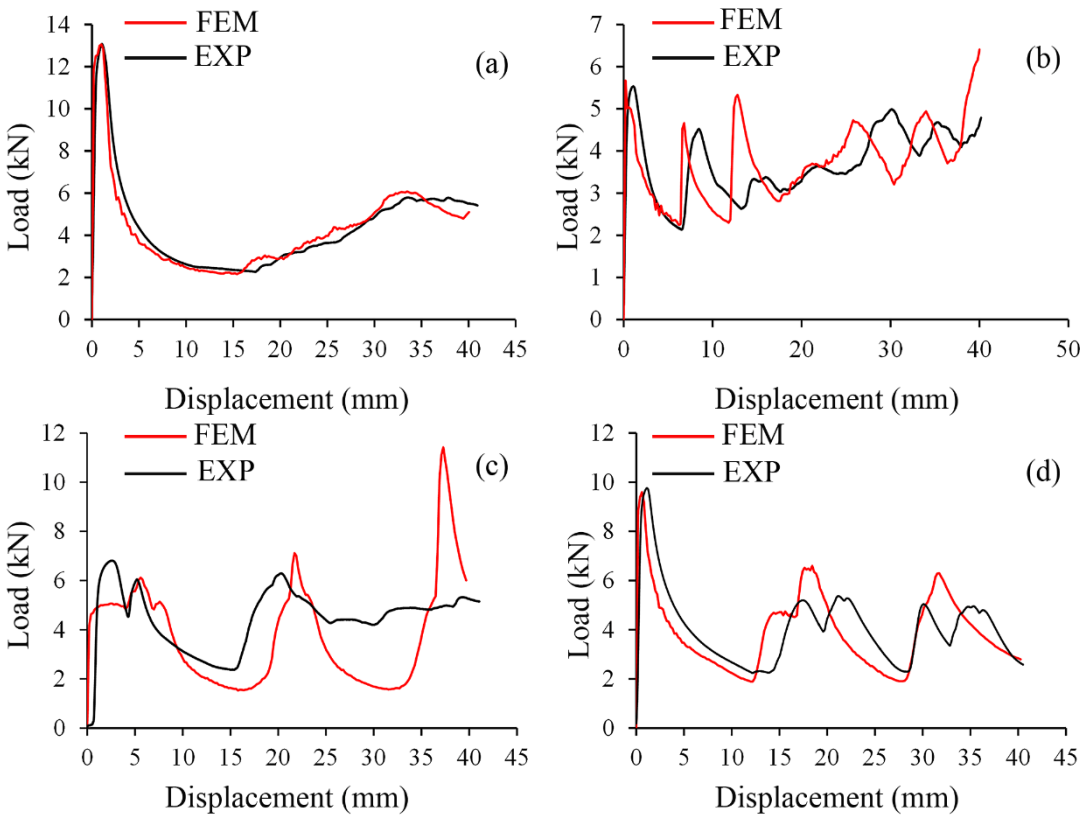

Fig. 21 Load-Displacement curves in quasi-static loading. (a) RE, (b) AR, (c) AC and (d) HO structures.

Table. 9
Summary of test results in quasi-static mode

Loading condition	specimen	Type of test	Mass (g)	PCF (kN)	MCF (kN)	CFE (%)	EA (J)	SEA (J/g)
Quasi-static	RE	Exp	51.73	13	4.34	33.3	175	3.38
		Num	52.5	13	4.29	33	173	3.32
		Error (%)	1	0	0.9	0.9	1	1
	AR	Exp	50.99	5.5	3.72	67.6	149.7	2.93
		Num	51.3	5.6	3.71	66.2	149.1	2.9
		Error (%)	0.6	1	0.2	0.5	0.4	1
	AC	Exp	51.68	6.4	4.5	70	180	3.48
		Num	50.42	6	3.85	64	154	3.05
		Error (%)	2	6	14	8	14	12
	HO	Exp	42	9.75	4	41	165	3.92
		Num	42.79	9.6	3.9	40	158	3.7
		Error (%)	1	1	2.5	2	4.2	5

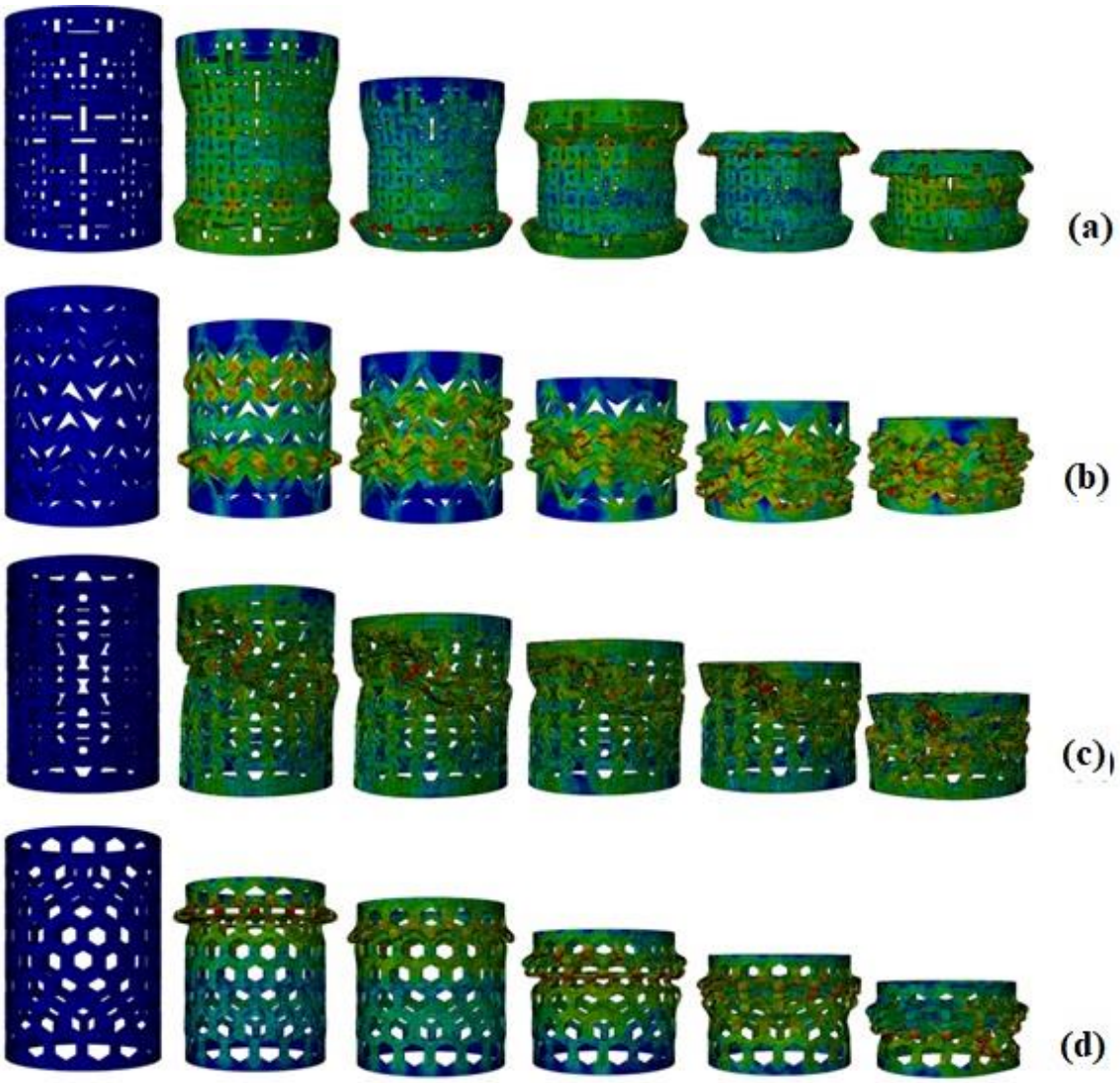

Fig. 22. The Collapse of auxetic structures in FE simulations, (a) AC, (b) AR, (c) RE and (d) HO

Fig. 23 shows that the initial collapse of the auxetic cells of RE, AC & AR tubes in the radial direction due to negative Poisson's ratio property inside the tube. At the same time, the HO structure expands outwards of the tube in the radial direction. From the deformed cross-sections of the structures, it can be seen that the cross-section of AC, AR & HO structures

had collapsed uniformly, while the collapsed RE structure's cross-sectional area is non-uniform and elliptical. It shows that this type of non-symmetric deformation affects the CFE specifically, that makes a considerable difference between PCF and MCF. However, it did not decrease the MCF and SEA, that these parameters for RE tubes are more than AR and in the same range for AC. Actually, it can be concluded from **Fig. 23** that the main factor for having a reticular tube with high MCF and SEA is that the diameter of the deformed tube does not changed so more. It can be easily seen in the **Fig. 23**. between AR and AC tubes.

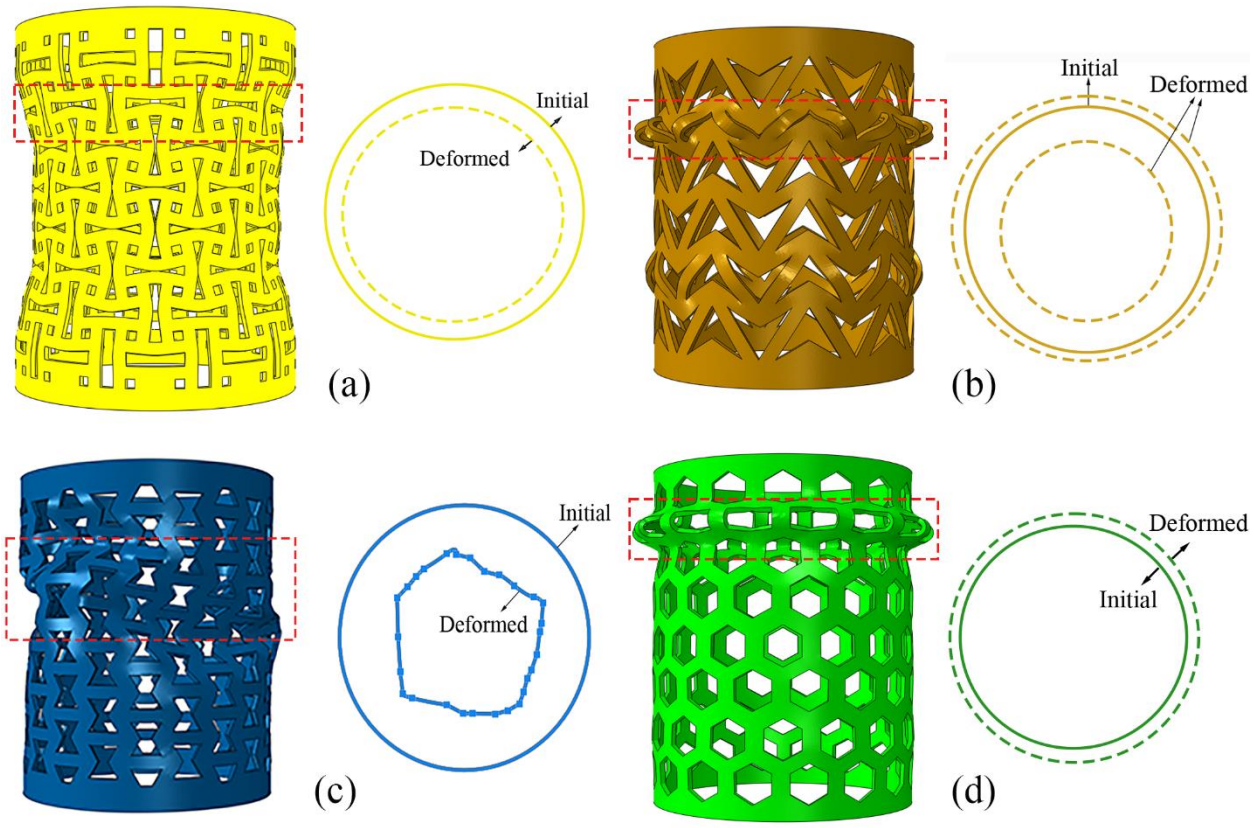

Fig. 23 Comparison of cross-sectional shapes in folding regions under quasi-static loading: (a) AC tube; (b) AR tube; (c) RE tube & (d) HO tube.

4.2 Effect of Loading Rate

The collapse mode of the structures at low velocity-impact conditions is shown in **Fig. 24**. It was observed that the deformation of the structures in the low-velocity impact mode was almost the same as the deformation in the quasi-static mode.

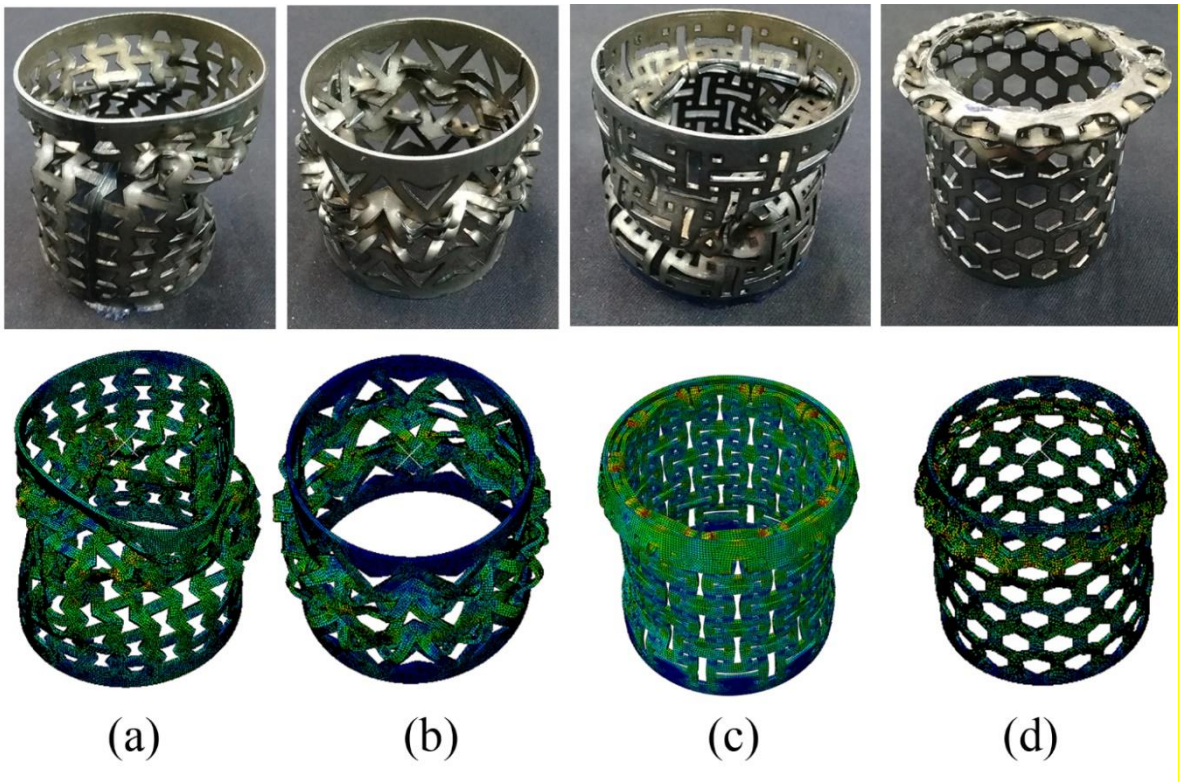

Fig. 24 Comparison of auxetic and non-auxetic tubes final deformation mode under Low-velocity impact loading: (a) RE, (b) AR, (c) AC and (d) HO structures.

The results of the main parameters are illustrated in **Fig. 25**. The maximum peak force (PCF) for the RE structure was about 17.37 KN and the maximum amount of energy absorption was 134 J for the AC structure. The results showed that the AR structure had the highest amount of crushing force efficiency (CFE) of about 62.65%. This value is 23.5%, 34.55, and 14.15% greater than the force crushing efficiency of HO, RE, and AC structures, respectively. The

maximum specific energy absorption was 2.63 for the AC auxetic tube that was more than the others. Considering this superiority of AC specimens in absorbing energy beside its good CFE, concluded it an excellent choice for energy absorber reticulated thin-walled tube. Comparing the results between quasi-static and low velocity impact shows that non-symmetric deformation of the RE tube had adverse effect on the energy absorption properties, that made it the worst tube with the least amount of SEA among the others.

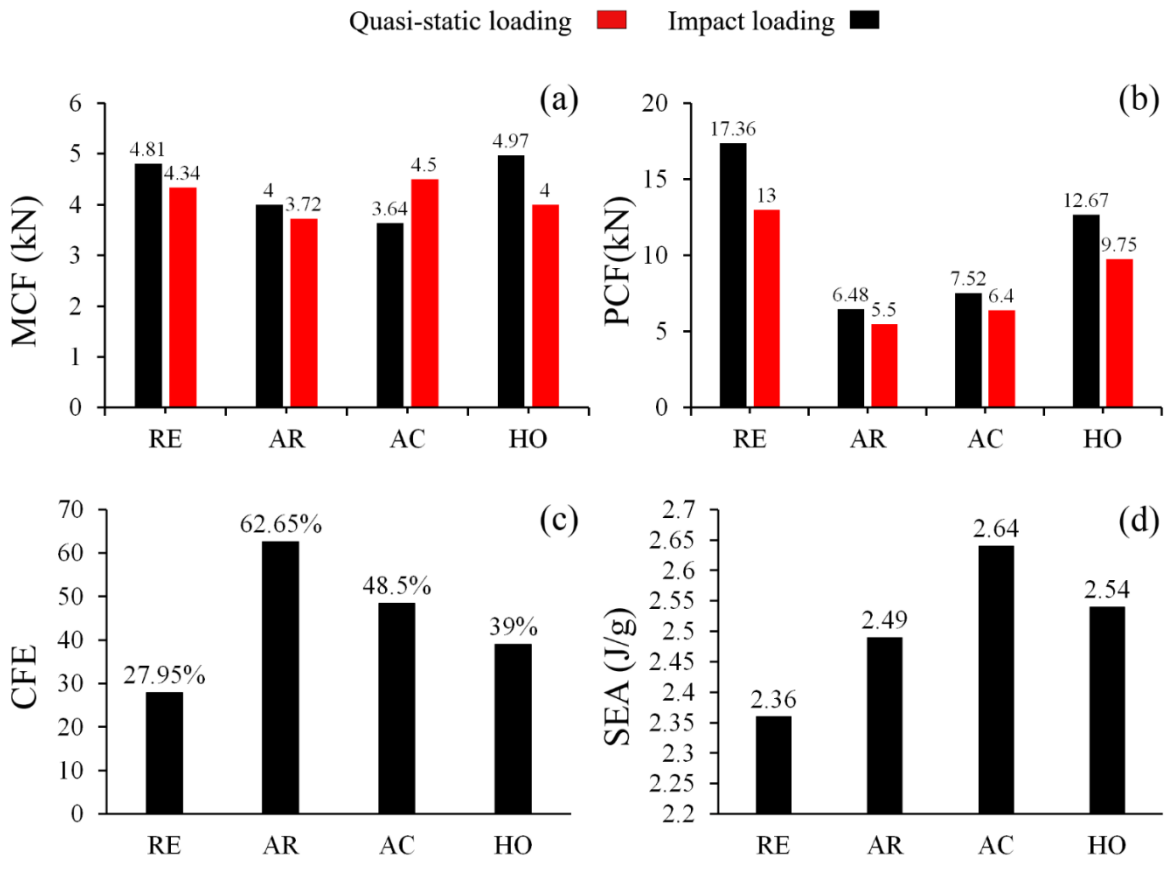

Fig. 25. A graphical comparison of MCF, PCF, CFE and SEA for structures: RE, AR, AC and HO structures in Low-velocity impact Loading condition.

According to the **Fig. 24 & 26**, the experimental and numerical tests are well matched. **Table. 10** summarized the comparison of compression indicators between numerical and

experimental results. It was observed that the load-displacement curves of the numerical test presented a similar trend with the experimental test. Errors between experimental and numerical results in PCF, MCF, CFE, EA and SEA parameters between 0.3-14, 3-14, 0.7-6, 0-5.3 and 0.7-6, respectively, which can be acceptable in engineering design and analysis. Defining the appropriate interaction conditions, mesh study, selecting the appropriate mesh size, and finding the values of Johnson-Cook equation for this study were effective parameters in the numerical simulation of experimental low-velocity impact tests in this study.

Table. 10
Summary of test results in low-velocity impact mode

Loading condition	specimen	Type of test	Mass (g)	PCF (kN)	MCF (kN)	CFE (%)	EA (J)	SEA (J/g)
Low- velocity impact	RE	Exp	52	16.44	4.69	29	124	2.39
		Num	52.5	18.04	4.85	27	121	2.3
		Error (%)	0.9	8	3	6	2.4	3
	AR	Exp	51	5.61	3.93	70	126	2.47
		Num	51.3	6.62	3.96	59.8	122	2.38
		Error (%)	0.5	14	0.7	14	3	3.6
	AC	Exp	51	7.55	3.6	48	133	2.6
		Num	50.42	6.87	3.86	56	140	2.77
		Error (%)	1	9	6	13	5	6
	HO	Exp	44	12.05	5.02	41	114	2.59
		Num	42.79	12.93	5.24	40	112	2.61
		Error (%)	2	6	4	2	1.7	0.7

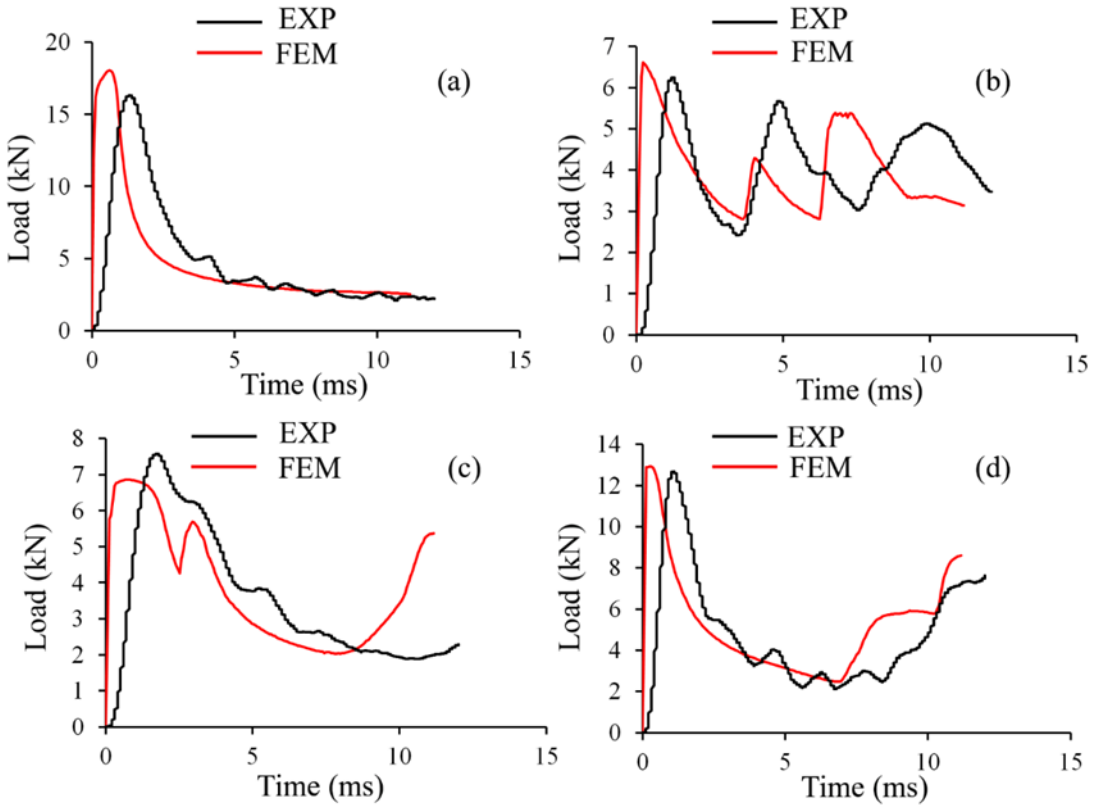

Fig. 26. Load-Time curves in Low-velocity impact condition for (a) RE, (b) AR, (c) AC and (d) HO structures.

In this section of study, after investigating the low-velocity impact response of RE, AR, AC and HO tubes in base strain rate on experimental procedure and validating FEM with the experimental results also comparing the results with quasi-static responses, the FE model for low-velocity impact loading was developed to determine the effect of higher strain rates, to this end, initial velocities equal to 4.9 m/s, 9.8 m/s and 19.6 m/s, was applied to the upper rigid platen. The crashworthiness parameters related to the numerical parametric study of low-velocity response were presented in **Table. 11**. The fold's pattern of AR, AC and HO tubes for altering different strain rates are seen to be similar to the pattern with a quasi-static

response. While, with increasing strain rate, the collapse pattern in RE tube changed from asymmetric to symmetrical (see **Fig. 27**)

Table. 11. Summary of the corresponding crashworthiness parameters of the tubes on various loading rates.

Structures	Initial velocity (m/s)	PCF(kN)	MCF(kN)	CFE%	EA(J)	SEA (J/gr)
RE	2.45	16.44	4.69	29	124	2.39
	4.9	19.13	5.12	27	235	4.52
	9.8	21.22	7.79	37	351	6.75
	19.6	21.52	7.79	37	351	6.75
AR	2.45	5.61	3.93	70	126	2.47
	4.9	6.98	4.55	65.1	205	4.02
	9.8	7.93	5.16	65	232.5	4.56
	19.6	8.08	5.98	74	269.5	5.29
AC	2.45	7.55	3.6	48	133	2.6
	4.9	7.24	4.86	67.1	219	4.3
	9.8	7.6	4.4	57.8	198.5	3.9
	19.6	8.24	5.6	67.9	252	4.95
HO	2.45	12.05	5.02	41	114	2.59
	4.9	13.86	4.72	34	212.5	4.82
	9.8	14.28	6	43.4	270	6.14
	19.6	15.08	5.82	38.5	261.9	5.95

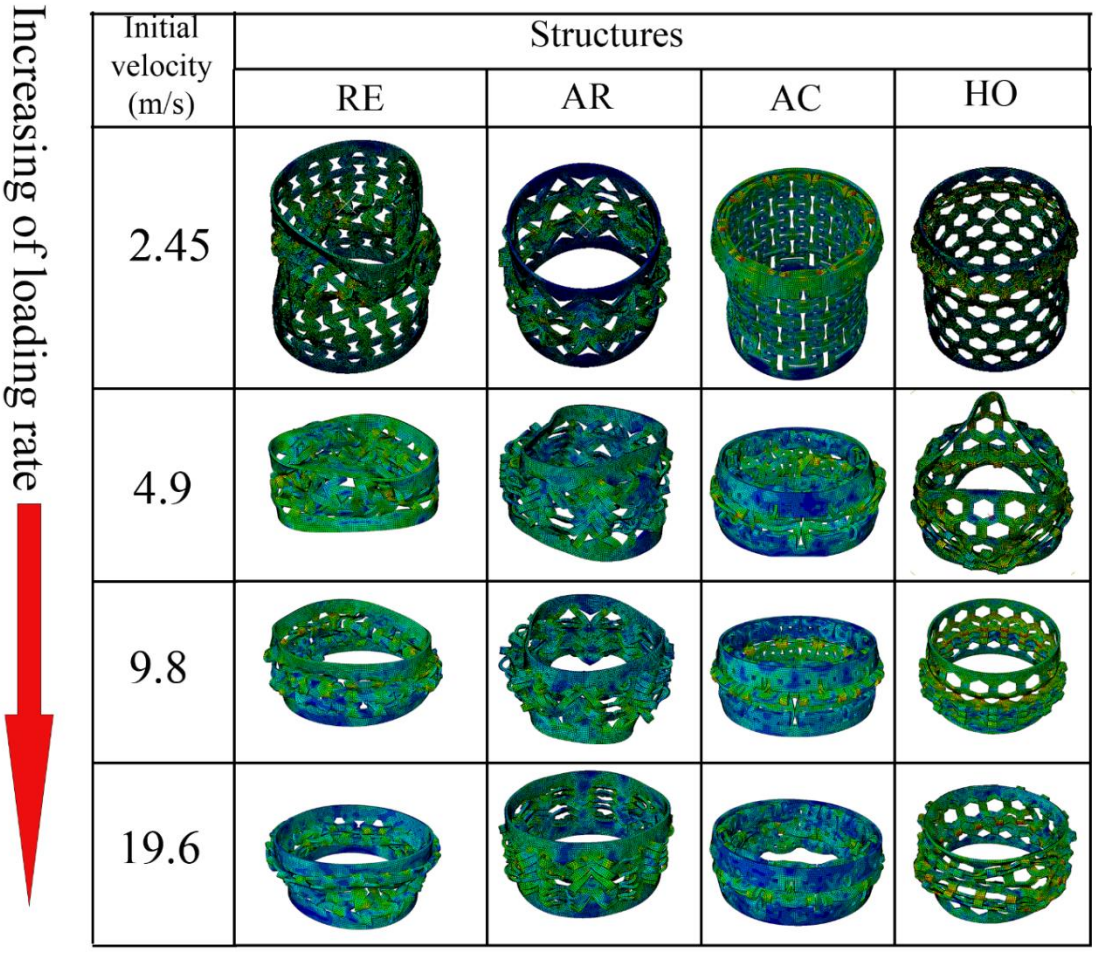

Fig. 27. final deformation mode of RE, AR, AC and HO structures under low-velocity impact loading with varying loading rates.

The influence of loading rate on PCF, MCF, EA and SEA of tubes is depicted in **Table. 11**. It was found that with the loading rate increasing, the PCF, MCF, EA and SEA of all tubes increased. In addition, with increasing of loading rate, the axial collapse behavior of RE structure changed from asymmetric to symmetrical, that was caused the RE structure showed the best performance in EA and SEA, in contrast, RE showed the worst

performance in CFE. The reason is that the high PCF in RE, which remarkably reduced the CFE of the tube. Moreover, comparing the extracted data for each tube under low-velocity impact with varied loading rate from **Table. 11.** Revealed increasing of the parameters of MCF, CFE, EA and SEA in the RE, AR and AC structures at the 19.8 m/s initial impact velocity compared to 2.45 m/s, this increasing of MCF, CFE, EA and SEA for RE, AR and AC structures respectively equal to (68%, 52% and 55%), (27%, 5% and 41%), (184%, 114% and 90%) and (184%, 114% and 90%). While in the HO structure, the difference of the parameters of MCF, CFE, EA and SEA at the 19.8 m/s initial impact velocity compared to 2.45 m/s respectively is 15%, -6%, 129% and 129%. It is concluded the increasing of loading rate in the auxetic tubes (RE, AR and AC structures) caused more collapse and so on the considerable increase in the MCF occurred. While in HO structure, caused more collapse but no considerable change in MCF. Therefore, it can be concluded that, in the higher loading rates, the RE structure had suitable crashworthiness indicators and integrity when crushed. The values of MCF, EA, and SEA of this auxetic tube indicated better crush integrity and energy absorption efficiency than could the conventional tube.

4.3 Effect of foam filling

One of the main advantages of filling the tubes used as energy absorbers in axial loading in this study, due to the interaction between the foam and auxetic tube, the pattern of RE structure folds was changed from asymmetric to axial symmetry, and the interaction in the AR, AC and HO tubes with foam caused the folds of the tubes to expand outwards. On this

basis, the reticulated tubes in this research were filled by Polyurethane foam and quasi-static axial compression tests were carried out. The patterns of folding and the load-displacement diagrams are shown in **Fig. 28 & 29**, respectively. According to the results, the folding pattern of the auxetic structures were became axisymmetric, especially for ARF and ACF structures that enhanced their energy absorbing capacity. On the other hand, the folding pattern of the HOF structure remain unchanged that shows that foam filling was not effective for this structure.

As shown in **Fig. 29**, the specific energy absorption (SEA) of REF structure was 5.12 J/g, that was more than the others and also showed a 52% increase compared to RE structure. This is the result of interaction between the foam and the tube. The greatest CFE value among the whole structure tested in the quasi-static state was for the ARF structure that was about 83.5 %. It is interesting to note that in the quasi-static loading of auxetic structures, the cross-section of the mentioned structures due to the auxetic property did not expand in the radial direction and collapsed unevenly. In contrast, the HOF non-auxetic structure, under quasi-static loading, expanded in the radial direction and while maintaining the circular cross-section and had a uniform collapse. Examination of the collapsed REF structure showed that the stiffening of auxetic cells occurred, while this stiffening was lower in the ARF and ACF structures. The foam as a filler in the auxetic tubes prevented these cells from shrinking into the tube and wasting energy by creating a reaction between the foam and the tube, friction and slip. It was observed that the REF auxetic tube, which had the highest cell stiffening under quasi-static loading, had the best performance in terms of specific energy absorption with a foam core.

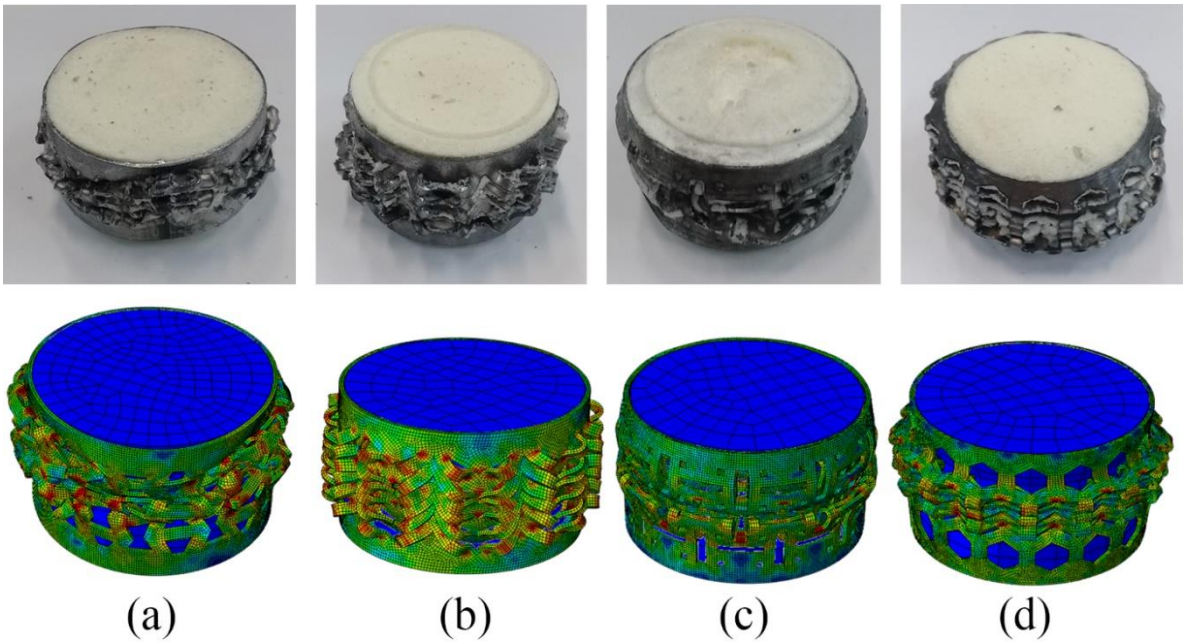

Fig. 28. Comparison of auxetic and non-auxetic tubes deformation mode under quasi-static loading: (a) REF, (b) ARF, (c) ACF and (d) HOF structures. (above images are experimental results and below images are numerical results).

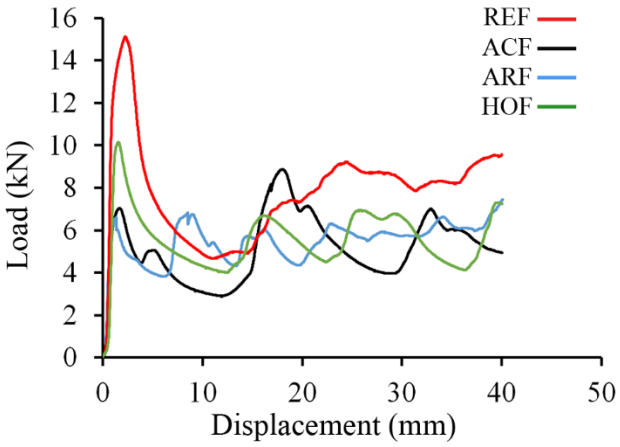

Fig. 29. Load-Displacement diagrams for REF, ARF, ACF and HOF structures in quasi-static Loading condition.

Fig. 30 shows the comparison of load-displacement curves and final deformation patterns of all studied structures between numerical and experimental results. It was observed that the numerical simulation presented a similar trend with the experimental test. Errors between experimental and numerical results in PCF, MCF, CFE, EA and SEA parameters for different structures are about 0.3-15, 0.2-14, 0.3-12, 0.4-14 and 0.9-12, respectively, which can be acceptable in engineering design and analysis. Good time scale, definition of appropriate interaction conditions, mesh study and selection of appropriate mesh size were effective parameters in numerical simulation of quasi-static experimental tests in this study.

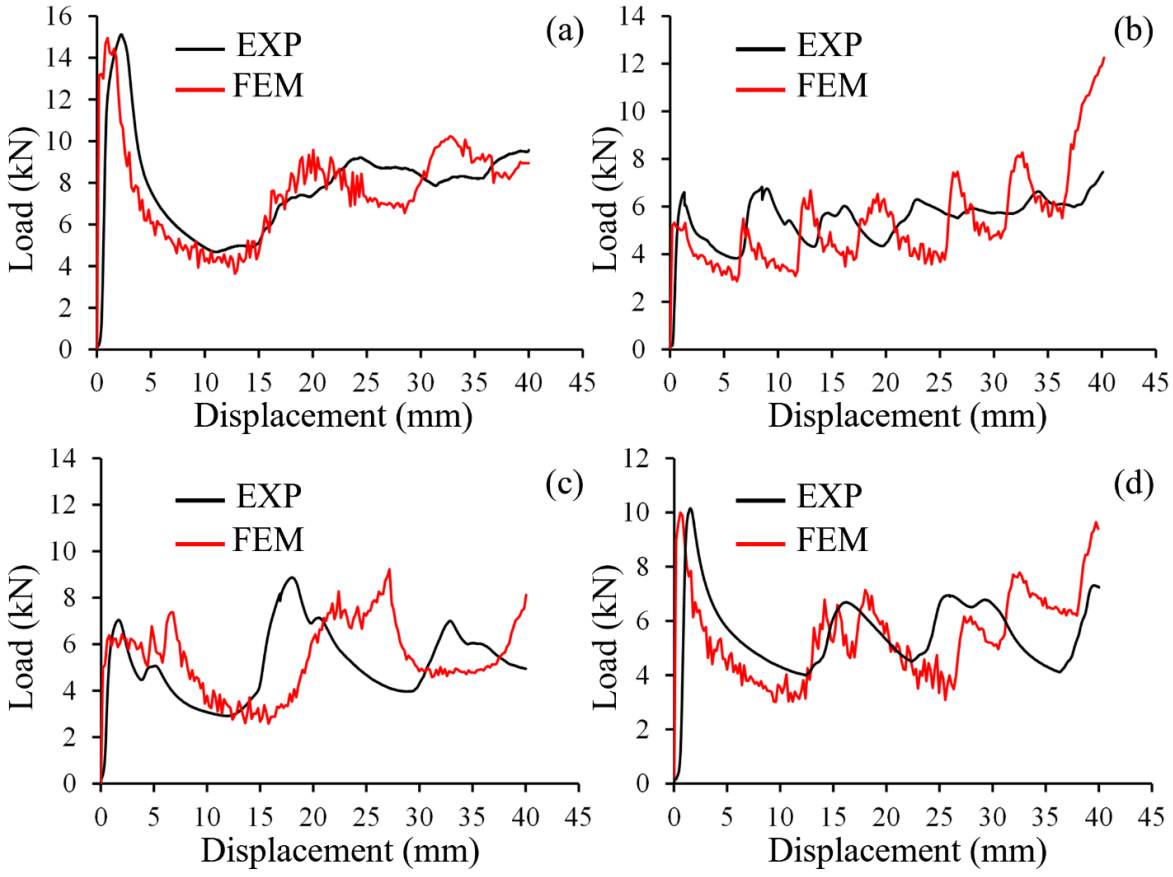

Fig. 30. Load-Displacement curves in quasi-static condition for (a) REF, (b) ARF, (c) ACF and (d) HOF structures.

Fig. 31 shows the comparison of final cross-sections of crushed empty and foam-filled tubes. It is clearly seen that filling the reticular tubes with foam, affected more on the structures that their wall moving inward like REF and ARF tubes. Moreover, filling with foam convert the non-symmetric deformation to symmetric deformation, specifically for REF structure. In HOF & ACF structures, there is not much modification in their final cross-section compared to their foamless state. The results show that the energy absorption in REF & ARF structures increased by 78% and 47% compared to structures RE and AR, respectively. While in HOF & ACF structures, the energy absorption was increased 30% and 13%, respectively compared to the empty tubes. This indicates that most of the energy absorption occurs due to the presence of foam in structures in which cell stiffening had occurred.

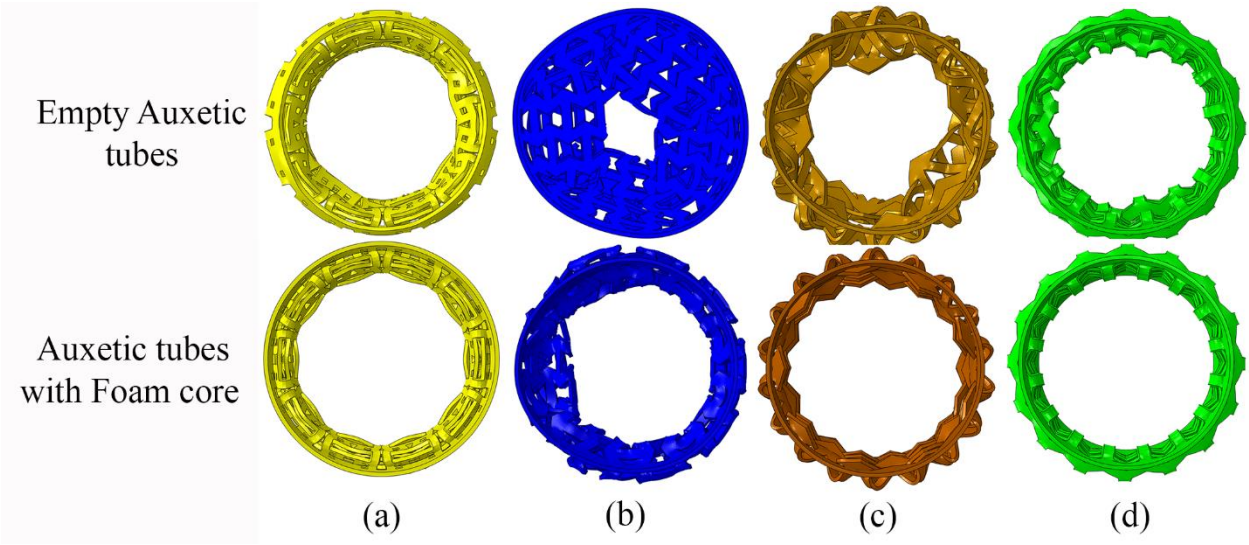

Fig. 31. Comparison of final cross-sectional shapes from top view under quasi-static loading: (a) AC & ACF tube; (b) RE & REF tube; (c) AR & ARF tube & (d) HO & HOF tube.

5 Conclusion

Efficient designs of hollow tubes structures are practicable if Novel porous units on the tube walls are adopted. In this study, the crushing response of novel hollow tubes with the hierarchical auxetic and non-auxetic units in the form of single and Foam- filled tubes are mainly investigated, to this end, the hollow single and Foam- filled tubes including RE, AR, AC, HO, REF, ARF, ACF, and HOF under quasi-static loading and RE, AR, AC and HO under low-velocity impact loading were investigated by experimental and numerical examination. For understanding the effects of the diverse loading rates of the energy absorption response of the RE, AR, AC and HO tubes, numerical parametric studies were conducted based on validating FE models versus the experimental results. The findings lead mainly to the following:

1- In the quasi-static state, auxetic structures have a higher amount of force-crushing efficiency (CFE) compared to the conventional non-auxetic structure. However, the non-auxetic HO structure had the most SEA.

2- In the low velocity-impact conditions, auxetic structures showed higher values of SEA, EA, and CFE compared to conventional non-auxetic structures.

3- It is concluded the increasing of loading rate in the auxetic tubes (RE, AR and AC structures) caused more collapse and so on the considerable increase in the MCF occurred. While in HO structure, caused more collapse but no considerable change in MCF. Therefore, it can be concluded that, in the higher loading rates, the RE structure had suitable crashworthiness indicators and integrity when crushed. The values of MCF, EA, and SEA of

this auxetic tube indicated better crush integrity and energy absorption efficiency than could the conventional tube.

4- The presence of foam-filler in auxetic tubes, considering that the collapse of RE auxetic structure was not uniform and in AR and AC, folding occurred with shrinking compared to HO conventional structure, caused the symmetry of deformation of REF structure during crushing and the interaction in the ARF, ACF and HOF tubes with foam caused the folds of the tubes to expand outwards. So, due to the excellent interaction between the foam and the tube's wall and symmetric wrinkling, the amount of specific energy absorption (SEA) increased more for the REF structure in comparison with the non-auxetic tube.

Conflict of Interest

The authors declare that they have no conflict of interest.

References:

[1] Q. Gao, X. Zhao, C. Wang, L. Wang, and Z. Ma, "Multi-objective crashworthiness optimization for an auxetic cylindrical structure under axial impact loading," *Materials and Design*, vol. 143, pp. 120–130, Apr. 2018, doi: 10.1016/j.matdes.2018.01.063.

[2] J. Zhang, G. Lu, and Z. You, "Large deformation and energy absorption of additively manufactured auxetic materials and structures : A review," *Composites Part B*, vol. 201, no. July, p. 108340, 2020, doi:

10.1016/j.compositesb.2020.108340.

[3] A. Ghamarian and S. Azarakhsh, “Axial crushing analysis of polyurethane foam-filled combined thin-walled structures : experimental and numerical analysis,” *International Journal of Crashworthiness*, vol. 24, no. 6, pp. 632–644, 2019, doi: 10.1080/13588265.2018.1506604.

[4] R. D. Hussein, D. Ruan, G. Lu, S. Guillow, and J. W. Yoon, “crossmark,” *Thin Walled Structures*, vol. 110, no. October 2016, pp. 140–154, 2017, doi: 10.1016/j.tws.2016.10.023.

[5] A. G. Hanssen, M. Langseth, and O. S. Hopperstad, “Static crushing of square aluminium extrusions with aluminium foam filler,” *International Journal of Mechanical Sciences*, vol. 41, no. 8, pp. 967–993, 1999, doi: 10.1016/s0020-7403(98)00064-2.

[6] T. Y. Reddy and R. J. Wall, “Axial compression of foam-filled thin-walled circular tubes,” *International Journal of Impact Engineering*, vol. 7, no. 2, pp. 151–166, 1988, doi: 10.1016/0734-743X(88)90023-1.

[7] A. Shiravand and M. Asgari, “Hybrid metal-composite conical tubes for energy absorption; theoretical development and numerical simulation,” *Thin-Walled Structures*, vol. 145, no. September, p. 106442, 2019, doi: 10.1016/j.tws.2019.106442.

[8] C. Ge, Q. Gao, and L. Wang, “Theoretical and numerical analysis of crashworthiness of elliptical thin-walled tube,” *International Journal of Mechanical Sciences*, vol.

148, pp. 467–474, 2018, doi: 10.1016/j.ijmecsci.2018.09.008.

[9] X. H. F. Yong Shen , Zhenyu Wu*, “Effect of reinforcement layer number on energy absorption of aluminum-CFRP hybrid square tubes under axial loading: Experimental and numerical study.” p. 155, 2020.

[10] V. H. Carneiro and H. Puga, “Axisymmetric auxetics,” *Composite Structures*, no. July, 2018, doi: 10.1016/j.compstruct.2018.07.116.

[11] Y. Guo *et al.*, “Deformation behaviors and energy absorption of auxetic lattice cylindrical structures under axial crushing load,” *Aerospace Science and Technology*, vol. 98, p. 105662, 2020, doi: 10.1016/j.ast.2019.105662.

[12] W. Lee *et al.*, “Effect of auxetic structures on crash behavior of cylindrical tube,” *Composite Structures*, vol. 208, pp. 836–846, Jan. 2019, doi: 10.1016/j.compstruct.2018.10.068.

[13] Q. Gao and W. H. Liao, “Energy absorption of thin walled tube filled with gradient auxetic structures-theory and simulation,” *International Journal of Mechanical Sciences*, vol. 201, no. May, p. 106475, 2021, doi: 10.1016/j.ijmecsci.2021.106475.

[14] N. Novak, M. Vesenjak, S. Tanaka, K. Hokamoto, and Z. Ren, “Compressive behaviour of chiral auxetic cellular structures at different strain rates,” *International Journal of Impact Engineering*, vol. 141, no. October 2019, 2020, doi: 10.1016/j.ijimpeng.2020.103566.

[15] H. Yin, G. Wen, Z. Liu, and Q. Qing, “Thin-Walled Structures Crashworthiness optimization design for foam- fi lled multi-cell thin-walled structures,” *Thin Walled*

Structures, vol. 75, pp. 8–17, 2014, doi: 10.1016/j.tws.2013.10.022.

[16] S. R. Guillow, G. Lu, and R. H. Grzebieta, "Quasi-static axial compression of thin-walled circular aluminium tubes," *International Journal of Mechanical Sciences*, vol. 43, no. 9, pp. 2103–2123, 2001, doi: 10.1016/S0020-7403(01)00031-5.

[17] X. Hou, Z. Deng, and K. Zhang, "Dynamic Crushing Strength Analysis of Auxetic Honeycombs," *Acta Mechanica Solida Sinica*, vol. 29, no. 5, pp. 490–501, 2016, doi: 10.1016/S0894-9166(16)30267-1.

[18] W. Liu, N. Wang, T. Luo, and Z. Lin, "In-plane dynamic crushing of re-entrant auxetic cellular structure," *Materials and Design*, vol. 100, pp. 84–91, 2016, doi: 10.1016/j.matdes.2016.03.086.

[19] X. Zhao, Q. Gao, L. Wang, Q. Yu, and Z. D. Ma, "Dynamic crushing of double-arrowed auxetic structure under impact loading," *Materials and Design*, vol. 160, pp. 527–537, 2018, doi: 10.1016/j.matdes.2018.09.041.

[20] K. P. Logakannan, V. Ramachandran, and J. Rengaswamy, "Mechanics of Materials Dynamic Performance of a 3D Re-entrant Structure," *Mechanics of Materials*, vol. 148, no. January, p. 103503, 2020, doi: 10.1016/j.mechmat.2020.103503.

[21] O. Mohammadiha and H. Ghariblu, "Crashworthiness study and optimisation of free inversion foam-filled tubes under dynamic loading," vol. 8265, no. September, 2017, doi: 10.1080/13588265.2017.1368119.

[22] Gibson, "The Royal Society is collaborating with JSTOR to digitize, preserve, and extend access to Proceedings of the Royal Society of London. Series A,

Mathematical and Physical Sciences. ® www.jstor.org," 1982.

[23] R. Lakes, N. Variability, A. Physcss, W. Meteorolgica, and O. Symposium, "Lakes1987-1," *Science*, vol. 235, no. 1987, pp. 1038–1041, 1987.

[24] S. Mohsenizadeh, R. Alipour, M. Shokri Rad, A. Farokhi Nejad, and Z. Ahmad, "Crashworthiness assessment of auxetic foam-filled tube under quasi-static axial loading," *Materials and Design*, vol. 88, pp. 258–268, 2015, doi: 10.1016/j.matdes.2015.08.152.

[25] X. Ren *et al.*, "Mechanical properties of foam-filled auxetic circular tubes: Experimental and numerical study," *Thin-Walled Structures*, vol. 170, no. November 2021, p. 108584, 2022, doi: 10.1016/j.tws.2021.108584.

[26] M. F. Guo, H. Yang, and L. Ma, "Design and analysis of 2D double-U auxetic honeycombs," *Thin-Walled Structures*, vol. 155, no. July, 2020, doi: 10.1016/j.tws.2020.106915.

[27] X. T. Wang, B. Wang, Z. H. Wen, and L. Ma, "Fabrication and mechanical properties of CFRP composite three-dimensional double-arrow-head auxetic structures," *Composites Science and Technology*, vol. 164, no. December 2017, pp. 92–102, 2018, doi: 10.1016/j.compscitech.2018.05.014.

[28] Q. Gao, W. H. Liao, and L. Wang, "On the low-velocity impact responses of auxetic double arrowed honeycomb," *Aerospace Science and Technology*, vol. 98, p. 105698, 2020, doi: 10.1016/j.ast.2020.105698.

[29] N. Novak *et al.*, "Crushing Behavior of Graded Auxetic Structures Built from

Inverted Tetrapods under Impact," *Physica Status Solidi (B) Basic Research*, vol. 256, no. 1, pp. 1–7, 2019, doi: 10.1002/pssb.201800040.

[30] M. Borovinšek, M. Vesenjak, K. Hokamoto, and Z. Ren, "An Experimental and Computational Study of the High-Velocity Impact of Low-Density Aluminum Foam," *Materials*, vol. 13, no. 8, p. 1949, Apr. 2020, doi: 10.3390/ma13081949.

[31] C. Luo, C. Z. Han, X. Y. Zhang, X. G. Zhang, X. Ren, and Y. M. Xie, "Design, manufacturing and applications of auxetic tubular structures: A review," *Thin-Walled Structures*, vol. 163, no. March, 2021, doi: 10.1016/j.tws.2021.107682.

[32] H. C. Luo *et al.*, "Mechanical properties of foam-filled hexagonal and re-entrant honeycombs under uniaxial compression," *Composite Structures*, vol. 280, p. 114922, Jan. 2022, doi: 10.1016/j.compstruct.2021.114922.

[33] F. H. Aboutalebi, M. Poursina, H. Nejatbakhsh, and M. Khataei, "Numerical Simulations and Experimental Validations of a Proposed Ductile Damage Model for DIN1623," *Engineering Fracture Mechanics*, 2017, doi: 10.1016/j.engfracmech.2017.12.041.

[34] ASTM E8, "ASTM E8/E8M standard test methods for tension testing of metallic materials 1," *Annual Book of ASTM Standards 4*, no. C, pp. 1–27, 2010, doi: 10.1520/E0008.

[35] N. V Gama, A. Ferreira, and A. Barros-timmons, "Polyurethane Foams: Past, Present, and Future," 2018, doi: 10.3390/ma11101841.

[36] Z. Nazari, H. Ahmadi, G. Liaghat, and S. Vahid, "Investigation on the compressive

properties of auxetic foams under different loading rates," *Polymer Engineering & Science*, Mar. 2022, doi: 10.1002/pen.25959.

[37] I. Nateghi-Boroujeni, G. Liaghat, and H. Ahmadi, "Experimental study on the effect of pentanediol as a chain extender on the mechanical properties of mdi polyurethane foams," *Iranian Journal of Polymer Science and Technology*, vol. 32, no. 4, pp. 317–326, 2019, doi: 10.22063/JIPST.2019.1679.

[38] F. O. R. Standardization and D. E. Normalisation, "International Standard Iso," vol. 1987, 1987.

[39] D. V. W. M. De Vries, "the Mechanics of Foam," no. July, p. 3, 2009.

[40] M. Najafi, H. Ahmadi, and G. Liaghat, "Experimental investigation on energy absorption of auxetic structures," *Materials Today: Proceedings*, vol. 34, pp. 350–355, 2021, doi: 10.1016/j.matpr.2020.06.075.

[41] D. Patidar and R. S. Rana, "ScienceDirect The effect of CO 2 laser cutting parameter on Mechanical & Microstructural characteristics of high strength steel-a review," *Materials Today: Proceedings*, vol. 5, no. 9, pp. 17753–17762, 2018, doi: 10.1016/j.matpr.2018.06.099.

[42] L. D. Scintilla, G. Palumbo, D. Sorgente, and L. Tricarico, "Fiber laser cutting of Ti6Al4V sheets for subsequent welding operations : Effect of cutting parameters on butt joints mechanical properties and strain behaviour," *Materials and Design*, vol. 47, pp. 300–308, 2013, doi: 10.1016/j.matdes.2012.12.014.

[43] A. Guerra and J. De Ciurana, "ScienceDirect ScienceDirect ScienceDirect

ScienceDirect Fibre laser cutting of polymer tubes for stents manufacturing Fibre laser cutting polymer tubes for stents manufacturing Costing models capacity optimization Trade-off," *Procedia Manufacturing*, vol. 13, pp. 190–196, 2017, doi: 10.1016/j.promfg.2017.09.038.

[44] M. Learning and R. Cookbook, *Shivdayal Rao, Abhijeet Sethi, Alok Kumar Das, Niladri Mandal, Kiran P, Rizul Ghosh, A.R. Dixit, A. Mandal*. .

[45] M. Murugesan and D. Jung, "Johnson Cook Material and Failure Model Parameters Estimation of AISI-1045 Medium Carbon Steel for Metal Forming Applications," *Materials*, vol. 12, no. 4, p. 609, Feb. 2019, doi: 10.3390/ma12040609.